nature portfolio

Peer Review File

Unassisted bipolar photoelectrochemical synthesis of H2O2

Corresponding Author: Professor Lei Wang

This file contains all reviewer reports in order by version, followed by all author rebuttals in order by version.

Version 0:

Reviewer comments:

Reviewer #1

(Remarks to the Author)
This manuscript makes a notable novel contribution to photoelectrochemical H2O2 synthesis through an innovative bias-free tandem PEC system, which combines a Zn-TiO2/BiVO4/WO3 photoanode (2e- WOR) and a Ru:CuO/Nb-CBO photocathode (2e- ORR). The work exhibits notable strengths as the dual-electrode design achieves an impressive total Faraday efficiency and stability, integrates comprehensive characterizations to elucidate reaction mechanisms, and validates practical applicability via natural sunlight tests and bacterial inactivation experiments. The experimental execution is rigorous. The strategy integrating heterojunction engineering, doping modification, and cocatalyst decoration is logically coherent. However, some aspects require improvement to deepen the mechanistic insight and complete the data. I recommend minor revision before publishing.
- For 20 cm2 scaled-up tests under natural sunlight, please provide average irradiance data and repeat the experiment at least 3 times to confirm consistency.
- Supplement photocurrent response data under different light intensities to simulate natural sunlight fluctuations and verify system stability under variable illumination.
- The authors have included Nyquist plots and their corresponding fitted circuits in the manuscript. To further clarify and make the impedance characteristics of the electrochemical system more accessible, it is recommended that detailed fitted impedance data be presented in tabular form within the information.
- How was the bactericidal experiment in Figure 4i conducted? The specific operational details need to be supplemented in the manuscript.
- It should add ICP-MS analysis of electrolytes after long-term stability tests to quantify possible dissolution of elements and verify material stability.
- It should supply time-resolved photoluminescence (TRPL) measurements to quantify charge carrier lifetime and further support claims of enhanced charge separation at photoanodes.
- With regard to unassisted tandem photoelectrochemical H2O2 synthesis, the authors should highlights the advance of bias-free tandem PEC system.
- This work presents the total faradaic efficiency exceeding 170%, thus, the authors could explain the superiorities of photocathode and photoanode by a bias-free photoelectrochemical bipolar system for efficient H2O2 production.

Reviewer #2

(Remarks to the Author)
This study reports an unassisted tandem photoelectrochemical system for hydrogen peroxide production by coupling two-electron water oxidation and two-electron oxygen reduction. A Zn–TiO2/BiVO4/WO3 photoanode with a type-II heterojunction achieves high selectivity for H_2O_2 generation by suppressing competing four-electron pathways, delivering a Faradaic efficiency of 90.2%. A Ru-decorated CuO/Nb–CuBi2O4 photocathode stabilizes *OOH intermediates and reaches a Faradaic efficiency of 91.9% with long-term stability. When integrated into a bias-free bipolar system, the device achieves a total Faradaic efficiency exceeding 170% and demonstrates scalable operation under natural sunlight using 20 cm2 electrodes. Overall, the catalyst characterization as well as the analyses of the WOR and ORR processes are thorough and well executed. However, major revisions are required to strengthen the originality, benchmarking, and scale-up relevance of this study.
1. A more in-depth discussion on the H2O2 production rate per unit area is required. Even when H2O2 is produced by coupling ORR and OER under an applied bias, significantly higher H2O2 production rates have been reported. Moreover,

recent studies have demonstrated H2O2 production without solar input, and the H2O2 production rates in those systems are expected to be even higher than those reported in this manuscript, particularly under 1 M NaOH conditions. Therefore, the novelty of the present work appears to be limited.
2. The WO3/BiVO4/TiO2 electrode configuration has already been reported in previous studies. The authors should clearly clarify how the present work differs from existing literatures.
3. In Figure 2, captions are provided for all panels except Figure 2c. A caption for panel (c) should be added.
4. In Figure 2h, the stability test is presented in a cyclic manner. When the experiment is conducted continuously for 10 hours, is the H2O2 produced via WOR decomposed by the catalyst? A discussion to address this issue is required.
5. For H2O2 quantification, the Ce4+ colorimetric method was employed. What is the R2 value of the standard calibration curve? In addition, Supplementary Figure 20b shows a standard curve measured over a concentration range of 0-400 μM. This range appears to be relatively high; is it appropriate to quantify low H2O2 concentrations using such a high-concentration calibration curve? Further clarification on the reliability of the H2O2 quantification method is needed.
6. In addition to ECSA, the authors should also provide BET surface area results. This is necessary to distinguish whether the increased ECSA originates from an increased number of active sites on the same geometric surface area, or simply from an increased geometric surface area.
7. The ORR saturation current density is typically around 5-6 mA cm-2 (based on RRDE measurements), which corresponds to near-complete consumption of dissolved oxygen supplied to the catalyst via electrode rotation. However, Figure 3e shows a current density exceeding this typical saturation value. What is the origin of this unusually high current density? Furthermore, why does the current density not reach saturation despite relying on dissolved oxygen?
8. The authors employed a photocathode-based PEC system, where ORR initiates at approximately 0.8 VRHE. Would it not be more effective to use an electrocatalyst instead of a PEC system (e.g., CuO, single-atom Co catalysts, O-CNTs)? Additionally, in a tandem PEC configuration, light transmitted through the photocathode is expected to reach the photoanode, leading to inevitable optical losses. In that case, would an electrocatalyst-based cathode not be more efficient than a photocathode?
9. The manuscript title includes the term “tandem PEC”. However, Figure 4a shows that the cathode and anode are spatially separated. Therefore, the use of the term “tandem PEC” appears to be inappropriate.
10. Please compare the current density obtained from the 20 cm2 electrode with that from lab-scale electrochemical measurements under 1 sun illumination. In addition, when scaling up to a large-area electrode, the authors should evaluate and report the electrode uniformity, for example by providing SEM images and XRD data from the corner, edge, and center regions.
11. Although a 20 cm2 electrode is described as a large-area system, this scale is still relatively small for meaningful scale-up demonstrations. The authors are encouraged to further increase the electrode size.
12. Please provide photographs of the actual experimental setup. Moreover, the experimental details should be described more explicitly, including parameters such as the solution volume of the cathode and anode.
13. The in-situ ATR-SEIRAS results support the authors’ claims well. However, this analysis does not provide information on where OOH is formed on the surface. If available, in-situ XANES or EXAFS results would allow more definitive identification of the active sites. If such analyses are challenging, are there alternative approaches to clearly verify that Zn, Ti, and Ru are the active sites?

Reviewer #3

(Remarks to the Author)
In this manuscript, the authors report a bias-free tandem photoelectrochemical (PEC) system for hydrogen peroxide (H_2O_2) production by integrating two-electron water oxidation ($2e^-$ WOR) at a Zn–TiO_2/$BiVO_4$/WO_3 photoanode with two-electron oxygen reduction ($2e^-$ ORR) at a Ru:CuO/Nb–CBO photocathode. The study demonstrates relatively high Faradaic efficiencies for both half-reactions, operation in an unassisted configuration, outdoor validation under natural sunlight, and bacterial inactivation tests. The manuscript is supported by extensive experimental characterization, in situ spectroscopy, and DFT calculations.

The work presents several strengths, particularly the integration of both half-reactions in a bias-free system and the breadth of mechanistic analysis. However, significant concerns remain regarding mechanistic clarity, interpretation of Faradaic efficiency values (especially total FE >100%), justification of material selection, and benchmarking against prior literature. In its current form, the conceptual rigor and critical analysis do not reach the level expected for publication in Nature Communications.

1. Insufficient mechanistic clarity regarding the role of Zn, Nb, and Ru

Although the authors attribute performance enhancement to heterojunction engineering and dopant effects, the mechanistic explanation remains largely qualitative and insufficiently substantiated.

The specific role of Zn incorporation in TiO_2 is not convincingly demonstrated. Is Zn acting as a shallow donor, modifying surface adsorption energetics, altering band bending, or passivating surface recombination sites? The evidence provided (minor XPS shifts, d-band center modulation in DFT) is indirect and does not clearly establish causal relationships with selectivity enhancement.

Similarly, the rationale for choosing Nb doping in CBO and Ru decoration on CuO/Nb–CBO lacks systematic justification. Why were these particular dopants selected over alternatives? Are there control experiments comparing different dopants or loadings?

The selectivity improvement is primarily explained by reduced impedance and increased electrochemical surface area. However, selectivity in multi-electron electrochemical reactions is governed by reaction pathway energetics and intermediate binding thermodynamics, not simply by reduced charge-transfer resistance or larger surface area. The current discussion does not sufficiently bridge kinetic observations with intrinsic catalytic selectivity.

A more rigorous structure–property–performance correlation is required to support the mechanistic claims.

2. Interpretation of Faradaic efficiency exceeding 100% requires careful reconsideration

The reported total Faradaic efficiency (FE) exceeding 170% in the unassisted system is conceptually problematic and requires substantially more rigorous explanation.

Reporting ~90% FE at both anode and cathode does not justify summing them to claim a “total FE” of ~170%. Faradaic efficiency is defined with respect to the charge passed in a given electrode process. Simply adding individual FEs risks double counting charge and may reflect misunderstanding of electron accounting in a closed circuit.

The manuscript does not clearly define how “total FE” is calculated in the unbiased configuration, nor does it provide a strict electron balance analysis.

If the anode and cathode each produce H_2O_2 independently in separated compartments, the correct interpretation should be clarified in terms of charge conservation and net reaction stoichiometry.

Because FE >100% contradicts fundamental electrochemical definitions unless carefully defined, this issue must be resolved rigorously. As it stands, it raises concerns about the validity of the quantitative analysis.

3. Benchmarking and literature comparison are not sufficiently fair or comprehensive

The manuscript compares its performance with selected prior reports; however:

There are published studies reporting higher half-reaction Faradaic efficiencies for both $2e^-$ WOR and $2e^-$ ORR individually. These are not adequately discussed.

The comparison does not consistently normalize parameters such as illumination intensity, electrolyte composition, applied bias, electrode area, or measurement duration.

Claiming “highest FE” without comprehensive benchmarking may be misleading.

A more balanced and quantitative comparison table, including half-cell and full-cell systems under equivalent conditions, is necessary to substantiate claims of advancement.

4. Overemphasis on impedance and ECSA as explanations for selectivity

Throughout the manuscript, performance improvements are frequently attributed to:

Reduced charge-transfer resistance (EIS),

Higher k_trans and lower k_rec (IMPS),

Increased electrochemical surface area (ECSA).

While these factors explain improved activity or stability, they do not inherently explain improved reaction selectivity between $2e^-$ and $4e^-$ pathways. Selectivity depends on relative free energy barriers of competing intermediates and their surface coverage dynamics.

Although DFT calculations are presented, the discussion remains descriptive rather than quantitative in linking calculated energetics to experimentally observed FE differences. The manuscript would benefit from:

A clearer energetic comparison between $2e^-$ and $4e^-$ limiting steps,

Correlation between ΔG differences and measured FE values,

Consideration of possible mass-transport or bicarbonate-mediated side reactions affecting quantification.

Reviewer #4

(Remarks to the Author)
This manuscript reports a photoelectrochemical bipolar system for hydrogen peroxide (H2O2) generation from water (H2O) and oxygen (O2), employing a Zn-TiO2/BVO/WO3 photoanode and a Ru:CuO/Nb-CBO photocathode. The work

demonstrates highly selective and stable H2O2 production using H2O and O2 as feedstocks.
The findings are highly interesting and novel, and the topic is well aligned with the scope of Nature Communications. However, several points require further clarification before the manuscript can be considered for publication.

・For Fig. 2 and Fig. 3, I believe that the selectivity (F. E.) data should include the applied charge or the reaction time in the captions.

・To demonstrate suppression of H2O2 decomposition, it is essential to provide long-term time-dependent data for both the anode and cathode reactions, including H2O2 production and selectivity (F. E.). In addition, I suggest including a control experiment (decomposition test) in which a high concentration of H2O2 is pre-added to evaluate its stability under the reaction conditions.

・In Fig. 2(a), the onset potentials for Zn-TiO2/BVO/WO3 and TiO2/BVO/WO3 are observed at more negative biases than +0.4 V vs. RHE (onset potential of +0.31 V vs. RHE in Zn-TiO2/BVO/WO3). Could the authors kindly clarify the reason for this behavior? If photoexcited electrons generated in BiVO4 are transferred to FTO through the conduction band of WO3, the onset potential would be expected to correspond to the conduction band minimum of WO3. How do the authors interpret the observed onset potentials in this context?

・In the mechanistic analysis in the main text, the high performance (high selectivity) of Zn-TiO2/BVO/WO3 is attributed to the strongest adsorption affinity of HCO4-. However, the reason why the two-electron oxidation of H2O2 (+0.68V vs. RHE), which is thermodynamically easier than the two-electron oxidation of H2O (+1.77V vs. RHE), is largely suppressed is not entirely clear to me. I would appreciate a more detailed explanation of the direct mechanism responsible for this suppression.

・It may strengthen the discussion to include citations on H2O2 generation via HCO3- oxidation, such as the following references.
K. Sayama et. al., Chem. Commun., 2016, 52, 5406-5409
K. Sayama et. al., Chem. Asian J., 2017, 12, 1111-1119
H. Kusama et. al., Phys. Chem. Chem. Phys., 2022, 24, 5894-5902

Reviewer #5

(Remarks to the Author)
In this manuscript, the authors report a well-designed bias-free PEC tandem system with impressive total FE (>170%) for H_2O_2 production. The integration of Zn–TiO_2/$BiVO_4$/WO_3 and Ru:CuO/Nb-CBO is scientifically sound, and the extensive in situ spectroscopic analysis convincingly supports the proposed mechanistic pathways. The authors provide strong evidence that heterojunction engineering and intermediate regulation suppress $4e^-$ pathways while stabilizing key *OOH species. However, several points require clarification: (1) The reported combined FE >170% should be explicitly discussed in terms of system-level accounting (dual-electrode contribution vs. theoretical limits). (2) Long-term stability beyond 10–50 h is still limited for practical deployment; degradation pathways should be analyzed. (3) The bicarbonate-mediated 2e WOR mechanism needs clearer differentiation between true catalytic pathways and solution-phase reactions. (4) Outdoor sunlight data would benefit from reporting irradiance variability. Thus, I would like to recommend the manuscript to be accepted after revision, and the authors should also address the following comments.

1. The authors are suggested to provide more information about the validation of the Ce^{4+} colorimetric H_2O_2 quantification against matrix effects (high carbonate/bicarbonate, high pH) and possible oxidants/reductants.

2. Regarding the mass balance and the crossover in the tandem cell, the authors should provide the detailed measurement of H_2O_2 crossover rate and any parasitic decomposition on the opposite electrode (with/without PEM). It would be good if the compartment concentrations vs time, membrane type/thickness can also be reported.

3. It is beneficial to show the system-level FE calculation (anode + cathode yields, charge passed at each electrode, normalization basis) and provide an error/uncertainty estimate. This would help to dismiss confusion about “exceeding 100%”.

4. It is recommended that the authors should have more insightful discussion on how they distinguish direct 2e WOR from bicarbonate-mediated solution pathways.

5. By evaluating the catalyst after 10–50 hours of electrolysis via ICP-MS, XPS, and electron microscopy, what evidence of degradation (e.g., leaching or cocatalyst detachment) becomes apparent? How do these physical changes explain the subsequent performance drift in terms of current and Faradaic Efficiency?

6. While outdoor field tests demonstrate stable FE, the resulting bulk concentrations remain in the micromolar range. To better contextualize these findings, please incorporate areal production rates and solar-to-chemical efficiency metrics. Furthermore, evaluate these results against application-specific benchmarks—such as the mg/L thresholds required for effective disinfection.

Version 1:

Reviewer comments:

Reviewer #1

(Remarks to the Author)
After the revision, this work could be accepted.

Reviewer #2

(Remarks to the Author)
General Comment: The authors have produced a novel bias-free tandem photoelectrochemical (PEC) system for sustainable hydrogen peroxide (H_2O_2) synthesis. By strategically integrating a Zn-TiO_2/$BiVO_4$/WO_3 photoanode and a Ru:CuO/Nb-CBO photocathode, the authors successfully elucidate the origin of highly selective H_2O_2 production, demonstrating how heterojunction engineering and precise element doping effectively suppress competing four-electron pathways and stabilize key *OOH intermediates. The impressive practical demonstrations, including a total Faradaic efficiency exceeding 160% in a scalable, membrane-free outdoor setup and its application for rapid bacterial inactivation, make this work highly commendable. This research is likely to capture the attention of a wide readership within the renewable energy and photoelectrocatalysis fields of the journal. Notwithstanding, to ensure acceptance, the authors need to deal with the following minor considerations:

Comment#1: The authors report onset potentials for BVO, BVO/WO_3, TiO_2/BVO/WO_3, and Zn-TiO_2/BVO/WO_3 ranging from 0.31 to 0.45 VRHE. However, the potential window selected for capacitance measurements (0.2 – 0.4 VRHE) overlaps with these Faradaic onset values. Since ECSA calculations must be conducted in a strictly non-Faradaic regime, this discrepancy may compromise the accuracy of the results. The authors should clarify this mismatch, re-evaluate their definition of onset potential, or adjust the potential window used for ECSA determination.

Comment#2: While the schematic in Fig. 4a and the scaled-up system are presented as membrane-less, the data for the small-scale system in Fig. 4c was obtained using a proton exchange membrane (PEM). To ensure the validity of the proposed membrane-free architecture, the authors need to provide stability data for the small-scale cells (1 and 2 cm^2) under membrane-less conditions, matching the setup of the scaled-up system and schematic illustration.

Comment#3: Despite the authors' efforts to suppress H_2O_2 degradation at both the photoanode and photocathode, H_2O_2 is inherently unstable due to its low thermodynamic barriers and facile kinetics toward both electrochemical oxidation and reduction. Given this bipolar instability, the system's ability to accumulate the product is likely limited. The authors should, therefore, determine the maximum attainable H_2O_2 concentration that this specific system can accommodate before decomposition rates offset production.

Comment#4: The statement “Gas chromatography measurements indicate that Zn-TiO_2/BVO/WO_3 exhibits the highest selectivity for H_2O_2 production at 0.6 VRHE, releasing the lowest amount of O_2 among these photoanodes” in page 8 is quite confusing because GC measures only O_2. Authors need to clarify this statement and indicate that FE of H_2O_2 plus O_2 equals ~100%.

Comment#5: There are typo. The authors need to correct it. For example: ‘selecitivities’ in page 9, ‘photoccathodes’ in page 25, ‘Ar2’, in Fig. S18.

Reviewer #3

(Remarks to the Author)
I appreciate the author's efforts for addressing all the comments raised during the review. no further comments.

Reviewer #4

(Remarks to the Author)
The authors have accurately revised the manuscript in accordance with the reviewer's comments. In addition, most of the reviewer's questions have been addressed in the revised version. Therefore, I feel that this manuscript has the potential to be published in Nature Communications.
However, I feel that it would be preferable to make the following minor revision:
· The authors should add the concentration (or amount) of the pre-added H_2O_2 (0.5 M) to the caption of the newly added Supplementary Fig. 43(c).

Reviewer #5

(Remarks to the Author)
The authors have carefully revised their manuscript according to the suggestions from the reviewers and addressed all the comments completely. After revision, the overall quality of the manuscript is improved and meets the standard, thus, I would

like to recommend the manuscript to be accepted for publication.

Version 2:

Reviewer comments:

Reviewer #2

(Remarks to the Author)
The authors have satisfactorily addressed all of concerns. Therefore, I recommend that the manuscript be accepted for publication

Reviewer #4

(Remarks to the Author)
Throughout the first and second rounds of review, the authors have carefully revised the manuscript in accordance with the reviewer's comments. In addition, most of the concerns raised by the reviewers have been addressed in the revised version. Therefore, I feel that that this manuscript is suitable for publication in Nature Communications.

Reviewer #1

We thank the reviewer 1 for the positive comments of our manuscript. We have made the suggested revision.

This manuscript makes a notable novel contribution to photoelectrochemical H_2O_2 synthesis through an innovative bias-free tandem PEC system, which combines a Zn-TiO_2/$BiVO_4$/WO_3 photoanode ($2e^-$ WOR) and a Ru:CuO/Nb-CBO photocathode ($2e^-$ ORR). The work exhibits notable strengths as the dual-electrode design achieves an impressive total Faraday efficiency and stability, integrates comprehensive characterizations to elucidate reaction mechanisms, and validates practical applicability via natural sunlight tests and bacterial inactivation experiments. The experimental execution is rigorous. The strategy integrating heterojunction engineering, doping modification, and cocatalyst decoration is logically coherent. However, some aspects require improvement to deepen the mechanistic insight and complete the data. I recommend minor revision before publishing.

1. For 20 cm^2 scaled-up tests under natural sunlight, please provide average irradiance data and repeat the experiment at least 3 times to confirm consistency.

Response: Thank you for your insightful comment. For the 20 cm^2 scaled-up tests under natural sunlight, we performed three independent repeated linear sweep voltammetry (LSV) and chronoamperometry (I-t) measurements, with a calibrated solar irradiance meter (LI-250A) real-time monitoring the illumination intensity (**Fig. R1**). The results show a significant positive correlation between the photocurrent density of the tandem system and the actual irradiance (R^2 = 0.996), confirming excellent reproducibility and reliability of the scaled-up system.

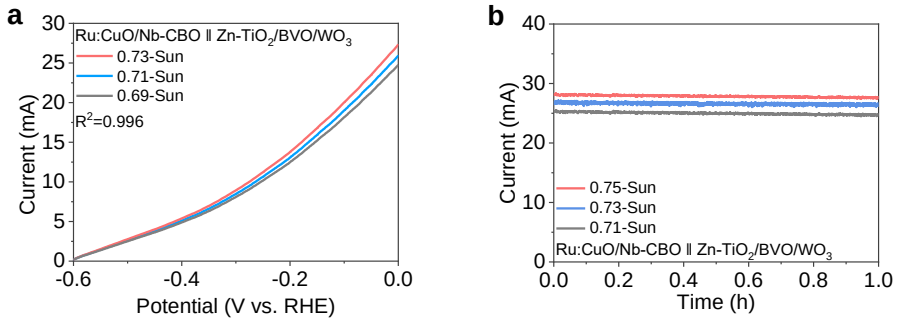

Fig. R1. a Three independent repeated LSV curves measured under different sunlight intensities. **b** Three independent repeated i-t curves measured under different sunlight intensities.

2. Supplement photocurrent response data under different light intensities to simulate natural sunlight fluctuations and verify system stability under variable illumination.

Response: Thank you for your valuable suggestion. To simulate natural sunlight fluctuations and validate the system's adaptability, we supplemented LSV and I-t measurements for the Zn-TiO_2/BVO/WO_3 photoanode, Ru:CuO/Nb-CBO photocathode, and 1 cm^2 unbiased tandem system under three representative light intensities (50, 75, 100 mW cm^{-2}) (**Fig. R2a-f**). All tests were conducted in 1 M $NaHCO_3$ + 1 M NaOH (pH=10), consistent with standard conditions. The results show the photoanode's photocurrent density reaches 0.98 mA cm^{-2} (50 mW cm^{-2}) at 0.6 V_{RHE}, 1.52 mA cm^{-2} (75 mW cm^{-2}), and 2.01 mA cm^{-2} (100 mW cm^{-2}) with a correlation coefficient R^2 of 0.998. The photocathode achieves 1.05 mA cm^{-2}, 1.63 mA cm^{-2}, and 2.14 mA cm^{-2} at the same potential with R^2=0.997. And the tandem system achieves 1.01 mA cm^{-2}, 1.54 mA cm^{-2}, and 2.10 mA cm^{-2} with R^2=0.999 at 0 V_{RHE}. All demonstrate reliable linear correlation with light intensity. Continuous 1 h I-t tests at each intensity confirm that all three components maintain over 98% of their initial current density without significant decay.

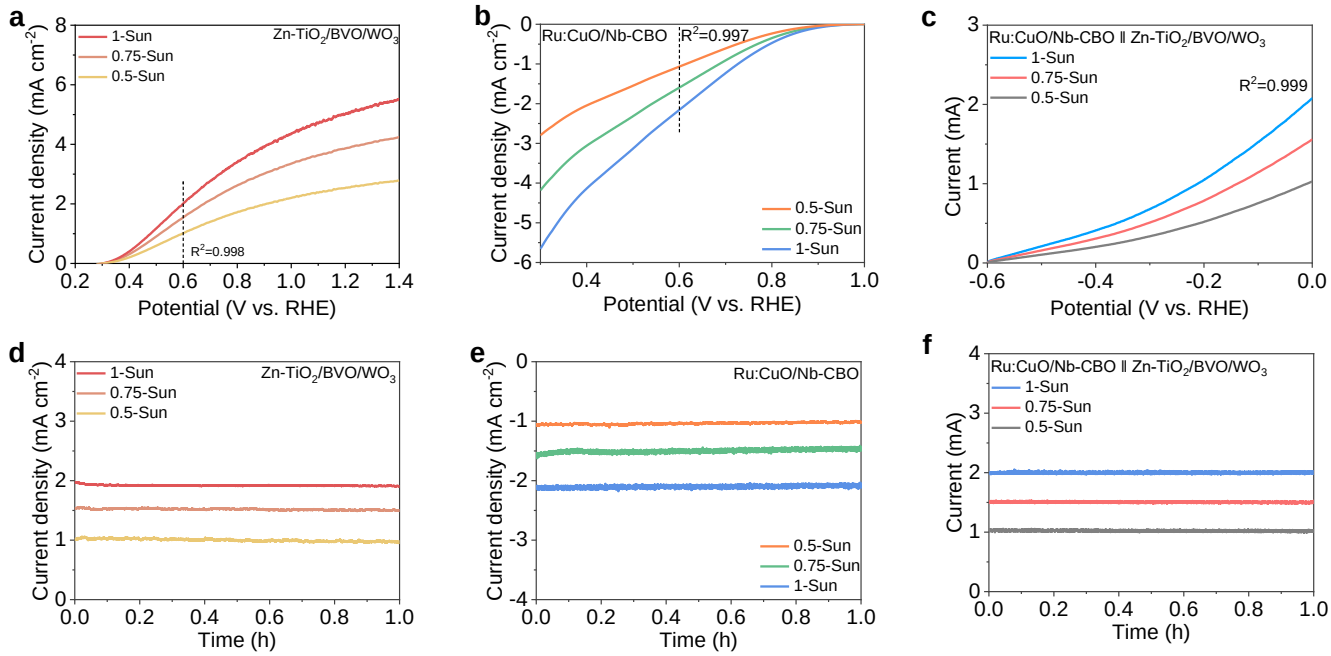

Fig. R2. a-c LSV curves of **a** Zn-TiO_2/BVO/WO_3, **b** Ru:CuO/Nb-CBO, and **c** unbiased tandem system with various light intensities. **d-f** I-t curves of **d** Zn-TiO_2/BVO/WO_3, **e** Ru:CuO/Nb-CBO, and **f** unbiased tandem system with various light intensities.

3. The authors have included Nyquist plots and their corresponding fitted circuits in the manuscript. To further clarify and make the impedance characteristics of the electrochemical system more accessible, it is recommended that detailed fitted impedance data be presented in tabular form within the information.

Response: Thank you for your constructive comment. We have collated the detailed fitted impedance parameters from the Nyquist plots into tabular form for clarity (**Tables R1 and R2**).

Table R1 Fitting results of the EIS for BVO, BVO/WO_3, TiO_2/BVO/WO_3, and Zn-TiO_2/BVO/WO_3 photoanodes.

Sample	R_s (Ω)	R_{trap} (Ω)	C_{bulk} ($\times10^{-6}$ F)	R_{ct} (Ω)	C_{ss} ($\times10^{-5}$ F)
BVO	48.27	423.8	4.82	348.5	1.357
BVO/WO_3	46.59	215.2	4.16	263.7	1.368
TiO_2/BVO/WO_3	41.25	248.1	3.97	232.4	1.649
Zn-TiO_2/BVO/WO_3	38.13	146.3	5.20	227.9	1.682

Table R2 Fitting results of the EIS for CBO, Nb-CBO, CuO/Nb-CBO, Ru:CuO/Nb-CBO photocathodes.

Sample	R_s (Ω)	R_1 (Ω)	CPE_1 ($\times10^{-6}$ F)	R_2 (Ω)	CPE_2 ($\times10^{-5}$ F)
CBO	35.45	183.5	3.84	199.5	1.34
Nb-CBO	31.24	146.8	3.25	176.8	1.67
CuO/Nb-CBO	36.78	134.5	3.67	186.7	1.95
Ru:CuO/Nb-CBO	33.61	167.4	3.45	169.5	1.88

4. How was the bactericidal experiment in Figure 4i conducted? The specific operational details need to be supplemented in the manuscript.

Response: Thank you for your careful comment. The tested strains were purchased as Escherichia coli (ATCC 25922) and Staphylococcus aureus (ATCC 25923) from a certified microbial resource center.[1] Pre-cultivation was performed by inoculating the strains into sterile Luria-Bertani (LB) medium and incubating at 37 °C for 12 h to reach the exponential growth phase. The bactericidal treatment was

carried out by mixing 1 mL of the pre-cultivated bacterial suspension with 9 mL of the PEC-generated electrolyte (which was adjusted from pH 10 to pH 7 using KH_2PO_4) at a volume ratio of 1:9, followed by incubation at 37 °C under dark conditions. This dark incubation was designed to exclude potential photodynamic effects. Sampling was performed at 20, 40, and 60 min after mixing. For each sampling time 100 μL aliquots of the mixture were serially diluted from 10^0 to 10^{-4} using sterile 0.9% NaCl solution and then spread evenly on LB agar plates. The plates were inverted and incubated at 37 °C for 24 h. After incubation colony-forming units (CFU) were counted to calculate the bacterial inactivation efficiency.[2]

References

[1] Jiang, C., Fei, Y.-F., Xu, W., Bao, Z., Shao, Y., Zhang, S., Hu, Z.-T., Wang, J. Synergistic effects of Bi_2O_3 and Ta_2O_5 for efficient electrochemical production of H_2O_2. *Appl. Catal. B.* **334**, 122867 (2023).

[2] Zhang, M.-D., Huang, J.-R., Liang, C.-P., Chen, X.-M., Liao, P.-Q. Continuous Electrosynthesis of Pure H_2O_2 Solution with MedicalGrade Concentration by a Conductive Ni-Phthalocyanine-Based Covalent Organic Framework. *J. Am. Chem. Soc.* **146**, 31034-31041 (2024).

5. It should add ICP-MS analysis of electrolytes after long-term stability tests to quantify possible dissolution of elements and verify material stability.

Response: Thank you for your valuable suggestion. We have performed ICP-MS analysis on the electrolytes after the long-term stability tests to quantify the dissolution of key elements and verify material stability (**Table R3**). For the Zn-TiO_2/BVO/WO_3 photoanode, which underwent 10 hours of continuous operation in 1 M $NaHCO_3$ (pH=10), measurable concentrations of Zn and Ti were detected, while the dissolution of V, Bi, and W remained below 0.05 mg/L. For the Ru:CuO/Nb-CBO photocathode that maintained stable operation for 50 hours in the same electrolyte, the dissolution concentrations of Ru and Cu were also found, whereas Nb and Bi were below 0.05 mg/L. These detectable dissolutions of Zn, Ti from the photoanode and Ru, Cu from the photocathode indicate that partial leaching of the Zn-TiO_2 and Ru:CuO components occurs during prolonged operation, which contributes to the gradual performance degradation observed in the stability tests.

Table R3 ICP analysis of electrolytes for Zn-TiO_2/BVO/WO_3 after 10 h i-t measurement and Ru:CuO/Nb-CBO after 50 h i-t measurement.

Sample	Zn (mg/L)	Ti (mg/L)	V (mg/L)	W (mg/L)	Bi (mg/L)	Cu (mg/L)	Ru (mg/L)	Nb (mg/L)
Zn-TiO_2/BVO/WO_3	0.17	0.38	0.03	0.01	0.03	---	---	---
Ru:CuO/Nb-CBO	---	---	---	---	0.02	0.34	0.18	0.03

6. It should supply time-resolved photoluminescence (TRPL) measurements to quantify charge carrier lifetime and further support claims of enhanced charge separation at photoanodes.

Response: Thank you for your insightful comment. We have supplemented time-resolved photoluminescence (TRPL) measurements for all photoanodes including BVO, BVO/WO_3, TiO_2/BVO/WO_3 and Zn-TiO_2/BVO/WO_3 to quantify charge carrier lifetime.[1] The TRPL decay spectra were fitted using a biexponential function, and the average charge carrier lifetime follows the order of Zn-TiO_2/BVO/WO_3 (0.88 ns) > TiO_2/BVO/WO_3 (0.87 ns) > BVO/WO_3 (0.84 ns) > BVO (0.83 ns) (**Fig. R3**). This extended lifetime of Zn-TiO_2/BVO/WO_3 confirms that Zn doping and type-II heterojunction engineering synergistically suppress charge recombination and enhance charge separation efficiency.

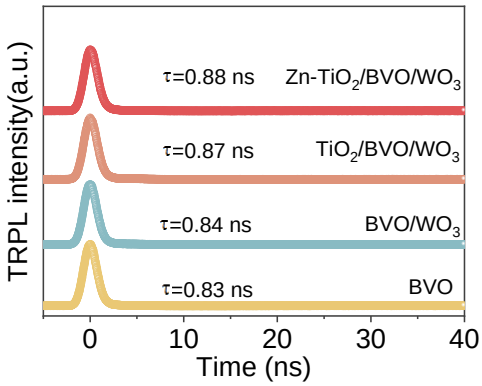

Fig. R3. TRPL decay spectra.

References

[1] Gao, R.-T., Gao, Z., Nguyen, N. T., Chen, J., Liu, X., Wang, L., Wu, L. Photoelectrochemical production of disinfectants from seawater. *Nat. Sustain.* **8**, 672-681 (2025).

7. With regard to unassisted tandem photoelectrochemical H_2O_2 synthesis, the authors should highlight the advance of bias-free tandem PEC system.

Response: Thank you for this valuable suggestion. We fully agree that emphasizing the advances of our bias-free tandem PEC system is critical to highlighting the novelty and practical significance of this work. We have supplemented a quantitative comparison table focusing on state-of-the-art bias-free tandem PEC systems for H_2O_2 production (**Table R4**). This table normalizes key parameters including operating stability, electrolyte environment, and total FE, clearly demonstrating that our work achieves competitive performance with the additional advantages of a membrane-free design and large-area (36 and 20 cm^2) outdoor adaptability. All revisions related to highlighting the advances of the bias-free tandem PEC system have been integrated into the revised manuscript.

Table R4 Summary of bipolar H_2O_2 performance of recently reported photoelectrodes under AM 1.5G illumination.

System	Sample	Applied bias (V_{RHE})	η_{H2O2} (μmol cm^{-2} min^{-1})	FE	Stability	Current density (mA cm^{-2})	Reference
PEC ‖ PEC	**Zn-TiO_2/BVO/WO_3‖ Ru:CuO/Nb-CBO ‖**	**unbiased**	**1.07**	**Total:163.37%**	**10 h**	**2.1**	**This work.**
PEC ‖ PEC	CPF-CzPB/Mo:$BiVO_4$ ‖ CPF-CzAD	unbiased	1.083	---	~168 h	1.85	Adv. Mater. 2025, 37, e08326
PEC ‖ PEC	$CaSnO_3$/SnO_2/$BiVO_4$ ‖ PV	unbiased	---	Photoanode:90 %	5 h	5.77	Adv. Energy Mater 2026, 16, e05447.
PEC ‖ EC	RuOx/TNR‖ AQ-graphite	unbiased	---	Total:90%	100 h	1.23	Energy Environ. Sci. 2021, 14, 3110.
PEC ‖ EC	P-Mo-BVO‖ AQ-CNT/C	unbiased	0.16	Photoanode:43 % Cathode:100%	5 h	---	Energy Environ. Sci. 2020, 13, 1730.

8. This work presents the total faradaic efficiency exceeding 170%, thus, the authors could explain the superiorities of photocathode and photoanode by a bias-free photoelectrochemical bipolar system for efficient H_2O_2 production.

Response: We thank the reviewer for the comment. The total FE exceeding 170 % originates from the synergistic combination of a highly selective photoanode for the $2e^-$ water oxidation reaction (WOR)

and a highly selective photocathode for the $2e^-$ oxygen reduction reaction (ORR).

The Zn-TiO_2/BVO/WO_3 photoanode employs a type-II heterojunction and Zn doping to suppress the *OOH intermediate, thereby favoring the $2e^-$ WOR over the competing $4e^-$ oxygen evolution reaction. It achieves a FE of 90.2% for H_2O_2 production at 0.6 V_{RHE} with a photocurrent density of 2.01 mA cm^{-2}. The Ru:CuO/Nb-CBO photocathode combines Nb doping, a CuO heterojunction and Ru cocatalyst decoration to stabilize the *OOH intermediate and promote the $2e^-$ ORR. It delivers a FE of 91.9% at the same potential with a photocurrent density of 2.14 mA cm^{-2} and maintains stable performance for over 50 hours.

When these two photoelectrodes are integrated into a bias free tandem cell, they share the same photogenerated charge flow. For each electron passing through the external circuit, the photoanode produces one H_2O_2 molecule via water oxidation and the photocathode produces another H_2O_2 molecule via oxygen reduction.[1] This concurrent production gives a theoretical maximum total FE of 200 %. Our measured total FE of 171.7% approaches this limit, demonstrating near optimal utilization of photogenerated charges. The two electrodes possess matched onset potentials, enabling the system to achieve a photocurrent density of 2.0 mA cm^{-2} under unbiased bias. This bipolar design thus offers a fundamental advantage over single electrode systems or systems that produce H_2O_2 at only one electrode.

Reference

[1] Wang, L., Wu, Y., Mao, S., Zhou, J., Zhang, Y., Zheng, X., Wu, X., Xu, H. Dual-Functional Catalyst of Amorphous TiO_2 Embedded in Mesoporous Carbon Hollow Spheres for H_2O_2 Electrosynthesis. *Adv. Mater.* **37**, e08326 (2025).

Reviewer #2:

We thank the reviewer 2 for the positive comments on our manuscript. We have made the suggested revision.

This study reports an unassisted tandem photoelectrochemical system for hydrogen peroxide production by coupling two-electron water oxidation and two-electron oxygen reduction. A Zn–TiO_2/$BiVO_4$/WO_3 photoanode with a type-II heterojunction achieves high selectivity for H_2O_2 generation by suppressing competing four-electron pathways, delivering a Faradaic efficiency of 90.2%. A Ru-decorated CuO/Nb–$CuBi_2O_4$ photocathode stabilizes *OOH intermediates and reaches a Faradaic efficiency of 91.9% with long-term stability. When integrated into a bias-free bipolar system, the device achieves a total Faradaic efficiency exceeding 170% and demonstrates scalable operation under natural sunlight using 20 cm^2 electrodes. Overall, the catalyst characterization as well as the analyses of the WOR and ORR processes are thorough and well executed. However, major revisions are required to strengthen the originality, benchmarking, and scale-up relevance of this study.

1. A more in-depth discussion on the H_2O_2 production rate per unit area is required. Even when H_2O_2 is produced by coupling ORR and OER under an applied bias, significantly higher H_2O_2 production rates have been reported. Moreover, recent studies have demonstrated H_2O_2 production without solar input, and the H_2O_2 production rates in those systems are expected to be even higher than those reported in this manuscript, particularly under 1 M NaOH conditions. Therefore, the novelty of the present work appears to be limited.

Response: We thank the reviewer for the comments. We agree that a more in-depth discussion of the per unit area production rate is needed, but we would like to clarify a key distinction. The high production rates reported in the literatures are mostly from electrocatalytic systems that consume external electrical energy. In contrast, our work is a bias-free photoelectrochemical (PEC) system that uses sunlight as the sole energy input with no external electricity. These two types of systems operate under fundamentally different energy paradigms.

1) Within the specific context of bias-free PEC systems, the production rate of 1.07 μmol cm^{-2} min^{-1} is competitive with recently reported systems of the same class (**Table R1**). More importantly, the novelty of this work is not limited to the production rate alone. A record total Faradaic efficiency

(FE) is achieved, approaching the theoretical maximum of 200% through concurrent H_2O_2 production at both electrodes. The inorganic heterojunction design provides excellent stability, with the photocathode operating for over 50 hours, outperforming most reported CBO-based photocathodes. The system is validated under natural sunlight using 20 cm^2 electrodes **without the use of electricity (applied bias)**, and direct disinfection application is demonstrated. Clear mechanistic insights are provided through combined in situ spectroscopy and DFT calculations.

We acknowledge that further improvement in production rate under bias-free conditions is desirable. We understand the reviewer's careful concern, and based on my experience, for future potential application, this set-up could be used in-house H_2O_2 production for sterilization, relying on solar energy without additional electricity. In the revised manuscript, we clarify the distinction between bias-free PEC and electrocatalytic systems, and include a comparison table with other bipolar H_2O_2 performance systems. We thank the reviewer for the constructive suggestion.

2) On the other side, considerable efforts have been made to develop more sustainable H_2O_2 production approaches (***Nature Materials*** 12 (2013) 1137; ***Science*** 351 (2016) 965; ***Science*** 366 (2019) 226; ***Nature Materials*** 18 (2019) 98; ***Nature Energy*** 8 (2023) 361; ***Nature Catalysis*** 7 (2024) 195). However, all above mentioned methods such as direct processing (using H_2 and O_2), photocatalysis, electrocatalysis, and mechanocatalysis require high energy inputs (e.g., light, electricity, and mechanical energy), complex processes, and **expensive catalysts** (e.g., Pd-based noble metals). Recently, rresearchers have reported that SnSe nanosheets with Sn vacancies catalyse H_2O_2 production from water and oxygen at ambient conditions (***Nature Catalysis*** 8 (2025) 465). This process can operate autonomously under ambient conditions (0 to 60 ˚C) solely driven by **thermal energy**.

Table R1 Summary of bipolar H_2O_2 performance of recently reported.

System	Sample	Applied bias (V_{RHE})	η_{H2O2} (μmol cm^{-2} min^{-1})	FE	Stability	Current density (mA cm^{-2})	Reference
PEC ‖ PEC	**Zn-TiO_2/BVO/WO_3‖ Ru:CuO/Nb-CBO ‖**	**unbiased**	**1.07**	**Total:163.37%**	**10 h**	**2.1**	**This work.**
PEC ‖ PEC	CPF-CzPB/Mo:$BiVO_4$ ‖ CPF-CzAD	unbiased	1.083	---	~168 h	1.85	Adv. Mater. 2025, 37, e08326

PEC ‖ PEC	$CaSnO_3/SnO_2/BiVO_4$ ‖ PV	unbiased	---	Photoanode:90%	5 h	5.77	Adv. Energy Mater. 2026, 16, e05447.
PEC ‖ EC	RuOx/TNR‖AQ-graphite	unbiased	---	Total:90%	100 h	1.23	Energy Environ. Sci. 2021, 14, 3110.
PEC ‖ EC	P-Mo-BVO ‖ AQ-CNT/C	unbiased	0.16	Photoanode:43% Cathode:100%	5 h	---	Energy Environ. Sci. 2020, 13, 1730.
EC ‖ EC	O-CNTs ‖ PTFE-C	1.7	24	Total:153%	~3 h	120	Nat. Catal. 2020, 3, 125.
EC ‖ EC	D-PSFZ ‖ D-PSFZ	2.1	---	Total:163%	100 h	50	Nat. Commun. 2023, 14, 5822.

2. The $WO_3/BiVO_4/TiO_2$ electrode configuration has already been reported in previous studies. The authors should clearly clarify how the present work differs from existing literatures.

Response: Thank you for your valuable comment. We appreciate the opportunity to clarify the core distinctions between our Zn-TiO_2/BVO/WO_3 photoanode and the previously reported $WO_3/BiVO_4/TiO_2$ configuration. Our work is not a simple reproduction but a targeted redesign and optimization for selective $2e^-$ WOR H_2O_2 production, with key differences as follows:

1) **Reaction orientation redefinition.** Prior $WO_3/BiVO_4/TiO_2$ structures were exclusively optimized for $4e^-$ WOR,[1,2] without the design for $2e^-$ WOR. Our work redevelops this trilayer structure as a selective $2e^-$ WOR photoanode. It achieves a H_2O_2 FE of 90.2% at 0.6 V_{RHE}. This has not been reported in previous studies of this configuration.

2) **Novel Zn doping engineering.** We introduce Zn doping into the TiO_2 layer. Zn doping optimizes heterojunction band alignment, improves photogenerated charge separation and transfer, and regulates *OOH intermediate adsorption, resulting in higher FEs than those of TiO_2/BVO/WO_3 without the induction of Zn (**Fig. 2b**). This modification stabilizes the $2e^-$ WOR pathway and limits H_2O_2 decomposition.

3) **Custom tandem system integration.** Our photoanode is not a separate electrode while it is designed to integrate with the Ru:CuO/Nb-CBO photocathode. This photocathode is used for selective $2e^-$ ORR. The integration helps to build a bias-free tandem PEC bipolar system. The system realizes synergetic H_2O_2 production through dual-electrode $2e^-$ WOR/ORR coupling under natural sunlight. Previous $WO_3/BiVO_4/TiO_2$ electrodes are only applied in single-electrode systems for water splitting

for O_2 evolution.

4) **Practical performance validation.** We tested the performance of our photoanode in 1 cm^2 lab-scale, 20 and 36 cm^2 scaled-up tandem systems under natural sunlight. We also verify its high stability. The dissolution of key elements is below the ICP-MS detection limit after long-term operation. Previous studies of this trilayer configuration seldom report scale-up tests, long-term stability evaluations and production validation under natural sunlight.

In summary, our work redefines the functional application of the $WO_3/BiVO_4/TiO_2$ trilayer structure. Zn doping modification, optimized heterojunction interface, selective $2e^-$ WOR design and integration into a bias-free tandem PEC system are the core innovations, which make our work different from existing reports of this electrode configuration. We also greatly appreciate the reported literatures, which has provided guidance and inspiration for our research.

References

[1] Kalanur, S. S., Yoo, I.-H., Park, J., Seo, H. Insights into the electronic bands of $WO_3/BiVO_4/TiO_2$, revealing high solar water splitting efficiency. *J. Mater. Chem. A* **5**, 1455 (2017).

[2] Park, E., Patil, S. S., Lee, H., Kumbhar, V. S., Lee, K. Photoelectrochemical H_2 evolution on $WO_3/BiVO_4$ enabled by single-crystalline TiO_2 overlayer modulations. *Nanoscale* **13**, 16932 (2021).

3. In Figure 2, captions are provided for all panels except Figure 2c. A caption for panel (c) should be added.

Response: Thank you for your careful comment. We have supplemented the caption for Figure 2c in the revised manuscript, - yield rates of H_2O_2 at various applied potentials. The captions of all figures in Figure 2 have been checked and standardized to ensure consistency and clarity.

4. In Figure 2h, the stability test is presented in a cyclic manner. When the experiment is conducted continuously for 10 hours, is the H_2O_2 produced via WOR decomposed by the catalyst? A discussion to address this issue is required.

Response: Thank you for your thoughtful and helpful comment. We have performed a 10 h continuous H_2O_2 accumulation test with the Zn-TiO_2/BVO/WO_3 photoanode under the reaction conditions (**Fig.R1a**). The experimental results show that the H_2O_2 yield can reach 300 μmol after the 10 h

accumulation test, and the FE remains relatively stable throughout the process. In addition, we have carried out parallel contrast experiments with and without the photoanode to verify the decomposition behavior of H_2O_2 (**Fig. R1b**).[1,2] The results demonstrate that the H_2O_2 concentrations in the two systems remain basically consistent after 10 h, which confirms that our photoanode does not induce H_2O_2 decomposition. The slight decrease in H_2O_2 concentration observed during the long-term reaction is caused by the spontaneous self-decomposition of H_2O_2 under the experimental conditions.

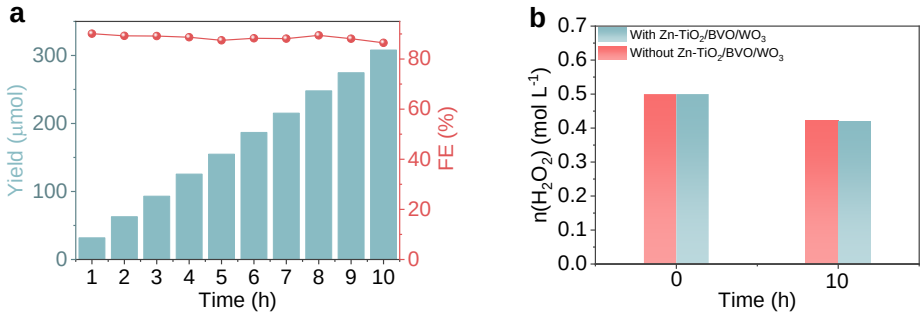

Fig. R1. a Accumulated H_2O_2 yields and FEs on Zn-TiO_2/BVO/WO_3 during 10 h operation. **b** The decomposition tests were carried out under identical experimental conditions with and without Zn-TiO_2/BVO/WO_3 photoanode.

References

[1] Wang, L., Wu, Y., Mao, S., Zhou, J., Zhang, Y., Zheng, X., Wu, X., Xu, H. Dual-Functional Catalyst of Amorphous TiO_2 Embedded in Mesoporous Carbon Hollow Spheres for H_2O_2 Electrosynthesis. *Adv. Mater.* **37**, e08326 (2025).

[2] Cheng, K., Ren, J., Wang, J., Muhammad, N., Chen, Y., Zhou, F., Guo, J., Duan, D., Li, T., Xu, B. The NiO hole transport layer between $BiVO_4$ and Ni_5P_4 for photoelectrochemical water oxidation to hydrogen peroxide. *Chem. Eng. J.* **510**, 161667 (2025).

5. For H_2O_2 quantification, the Ce^{4+} colorimetric method was employed. What is the R^2 value of the standard calibration curve? In addition, Supplementary Figure 20b shows a standard curve measured over a concentration range of 0-400 μM. This range appears to be relatively high; is it appropriate to quantify low H_2O_2 concentrations using such a high-concentration calibration curve? Further clarification on the reliability of the H_2O_2 quantification method is needed.

Response: Thank you for your constructive comment. We highly appreciate the valuable suggestion on the reliability of the Ce^{4+} colorimetric method for H_2O_2 quantification, and we have carried out targeted optimization and verification experiments to address the raised concerns.

1) Appropriateness of the concentration range for low H_2O_2 quantification. In our unbiased

PEC system, the H_2O_2 concentrations generated in the electrolyte typically range from approximately 5 μM to 350 μM, depending on the reaction time and electrode area. Therefore, the 0-400 μM calibration curve fully covers the entire range of our measured sample concentrations. For samples with very low concentrations (e.g., below 10 μM), the absorbance values still fall on the linear portion of the calibration curve with sufficient sensitivity. To further validate the reliability at low concentrations, we have prepared an additional low-concentration calibration curve in the range of 0-100 μM (R^2 = 0.997) (**Fig.R2a and 2b**).

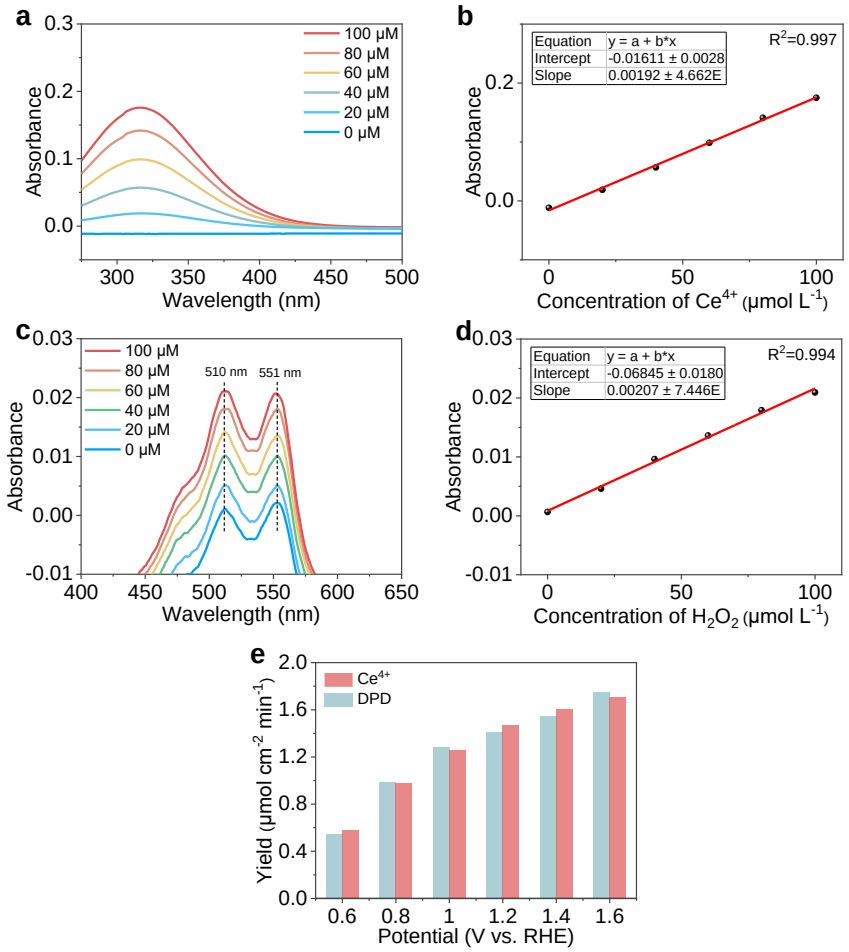

Fig. R2. a UV-visible absorption spectra for various Ce^{4+} concentrations. **b** Fitting results of the absorbance vs. concentration. **c** The base of verification using standard 0 to 100 μM H_2O_2. **d** Fitting results of the absorbance vs. concentration. **e** Yield rates of H_2O_2 at various applied potentials using the N,N-diethyl-p-phenylenediamine (DPD) colorimetric method and the Ce^{4+} method.

2) Reliability of the quantification method. The Ce^{4+} colorimetric method is well established for H_2O_2 detection in photoelectrochemical and electrocatalytic systems.[1,2] In addition, selected

samples were cross-checked using the N,N-diethyl-p-phenylenediamine (DPD) colorimetric method, and the results agreed within ±5% of the Ce^{4+} method (**Fig.R2c-e**).[3,4]

References

[1] Sun, Y., Fan, K., Wang, L., Yang, Y., Li, Z., Shao, M., Duan X. Boosting electrochemical oxygen reduction to hydrogen peroxide coupled with organic oxidation. *Nat. Commun.* **15**, 6098 (2024).

[2] Yan, M., Yang, H., Gong, Z., Zhu, J., Allen, C., Cheng, T., Fei, H. Sulfur-Tuned Main-Group Sb−N−C Catalysts for Selective 2-Electron and 4-Electron Oxygen Reduction. *Adv. Mater.* **36**, 2402963 (2024).

[3] Moon, S., Park, Y. S., Lee, H., Jeong, W., Kwon, E., Lee, J., Yun, J., Lee, S., Kim, J. H., Yu, S., Moon, J. Unassisted photoelectrochemical hydrogen peroxide production over MoO_x-supported Mo on a Cu_3BiS_3 photocathode. *Energy Environ. Sci.* **17**, 5588 (2024).

[4] Mehrotra, R., Oh, D., Jang, J.-W. Unassisted selective solar hydrogen peroxide production by an oxidised buckypaper-integrated perovskite photocathode. *Nat. Commun.* **12**, 6644 (2021).

6. In addition to ECSA, the authors should also provide BET surface area results. This is necessary to distinguish whether the increased ECSA originates from an increased number of active sites on the same geometric surface area, or simply from an increased geometric surface area.

Response: Thank you for your constructive comment. We have supplemented the Brunauer-Emmett-Teller (BET) specific surface area measurements for all photoanodes and photocathodes samples. The results clearly distinguish the intrinsic origin of the enhanced electrochemical surface area (ECSA) in our designed electrodes.

For the Zn-TiO_2/BVO/WO_3 photoanode, the measured BET specific surface area is 4.58 $m^2\ g^{-1}$, which shows only a slight increase compared with TiO_2/BVO/WO_3 (3.789 $m^2\ g^{-1}$) and pristine BVO (3.576 $m^2\ g^{-1}$). In sharp contrast, the ECSA of Zn-TiO_2/BVO/WO_3 reaches 15.26 μF cm^{-2}, which is 1.22 times that of TiO_2/BVO/WO_3 (12.58 μF cm^{-2}) and twice that of pristine BVO (7.6 μF cm^{-2}). For the Ru:CuO/Nb-CBO photocathode, its BET specific surface area is 7.589 $m^2\ g^{-1}$, with a negligible increase compared with CBO (6.583 $m^2\ g^{-1}$), while its ECSA is 5.73 μF cm^{-2}, 2.5 times that of pristine CBO (2.27 μF cm^{-2}).

These BET results confirm that the geometric surface areas of our optimized electrodes have no significant expansion. The remarkable enhancement of ECSA is therefore not caused by the increase

of geometric surface area, but solely attributed to the increased number of electrochemical active sites on the same geometric surface area.

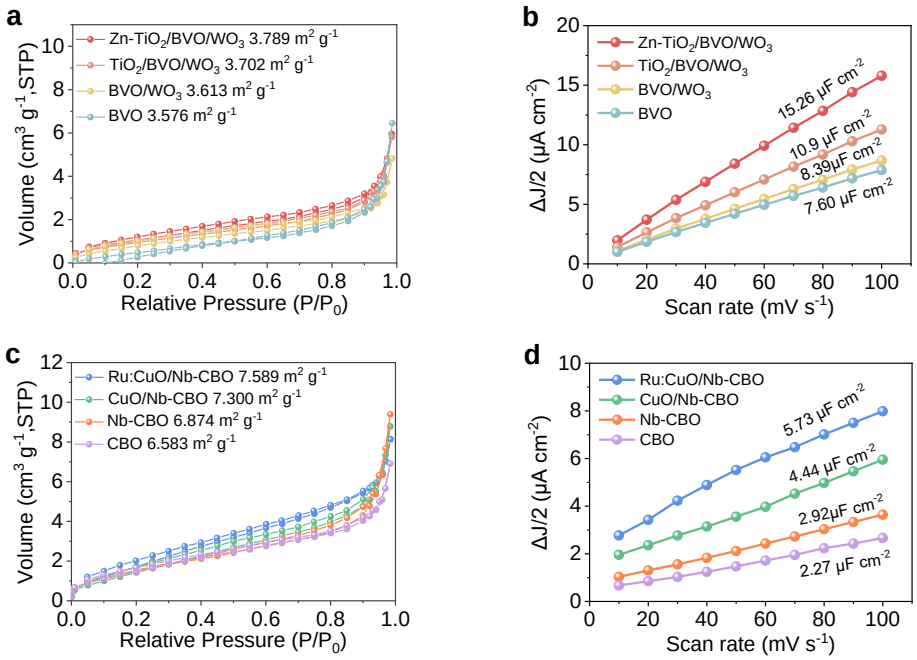

Fig. R3. a N_2 adsorption-desorption isotherms of various photoanodes. **b** Linear relationship of electrochemical surface areas for various photoanodes. **c** N_2 adsorption-desorption isotherms of various photocathodes. **d** Linear relationship of electrochemical surface areas for various photocathodes.

7. The ORR saturation current density is typically around 5-6 mA cm^{-2} (based on RRDE measurements), which corresponds to near-complete consumption of dissolved oxygen supplied to the catalyst via electrode rotation. However, Figure 3e shows a current density exceeding this typical saturation value. What is the origin of this unusually high current density? Furthermore, why does the current density not reach saturation despite relying on dissolved oxygen?

Response: Thank you for your insightful comment. We appreciate the opportunity to clarify the origin of the measured current density and the absence of the typical saturation phenomenon in our PEC ORR tests, which stems from the fundamental difference in test systems and the determining factors of saturation current density between our photocathode measurements and conventional RRDE tests, with detailed explanations as follows.

The photoelectrochemical ORR tests for the Pd:CuO/W-CBO photocathode were conducted in a non-RRDE configuration. Conventional RRDE tests report a saturation current density of ~5-6 mA cm^{-2} for ORR, which is strictly limited by the mass transfer rate of dissolved oxygen to the catalyst

surface driven by electrode rotation. In contrast, the saturation current density of our FTO-clamped photocathode in PEC ORR tests is not governed by dissolved oxygen mass transfer, but is solely determined by the intrinsic photoelectrochemical properties of the $CuBi_2O_4$ (CBO) semiconductor.[1,2] CBO is a p-type semiconductor with an optimal bandgap of 1.5~1.8 eV for visible light absorption. Based on the bandgap characteristics and the theoretical calculation of semiconductor photogenerated carrier yield under AM 1.5G illumination (100 mW cm^{-2}), the intrinsic theoretical saturation photocurrent density of CBO is calculated to be ~19.7 mA cm^{-2}. The current density of ~6 mA cm^{-2} observed at 0.3 V_{RHE} in Figure 3e is located in the range of theoretical saturation value. The absence of a current saturation platform in the test curve is because the measured current density is still in the ascending range of the CBO semiconductor's intrinsic photocurrent and has not yet reached its theoretical saturation value, which is the essential reason why the current density does not show the saturation phenomenon observed in RRDE tests. We really thank you for your comments.

References

[1] Zhang, Z., Chen. X., Hao, R., Feng, Q., Xie, E. Van Der Waals Heterojunction Modulated Charge Collection for H_2O_2 Production Photocathode. *Adv. Funct. Mater.* **33**, 2303391 (2023).

[2] Sun, M., Liu, B., Han, W., Zhang, Z., Xie, M. $CuBi_2O_4$ photocathode with integrated electric field for enhanced H_2O_2 production. *Appl. Catal. B.* **304**, 120980 (2022).

8. The authors employed a photocathode-based PEC system, where ORR initiates at approximately 0.8 V_{RHE}. Would it not be more effective to use an electrocatalyst instead of a PEC system (e.g., CuO, single-atom Co catalysts, O-CNTs)? Additionally, in a tandem PEC configuration, light transmitted through the photocathode is expected to reach the photoanode, leading to inevitable optical losses. In that case, would an electrocatalyst-based cathode not be more efficient than a photocathode?

Response: Thank you for your thoughtful and professional questions regarding the selection of photocathode over electrocatalytic cathode and the concern of optical loss in the tandem PEC configuration. We greatly appreciate these constructive points and provide detailed justifications, as follows:

1) Electrocatalysts are known to achieve high current densities for the two-electron oxygen reduction reaction ($2e^-$ ORR) under applied bias. However, one key factor in this comparison is the

thermodynamic limitation of the $2e^-$ ORR. The standard reduction potential for the $2e^-$ ORR to H_2O_2 is approximately 0.76 V vs. RHE under neutral/alkaline conditions.[1,2] Due to this thermodynamic ceiling, even the most active $2e^-$ ORR electrocatalysts typically show a sharp decline in FE when the applied potential exceeds 0.7 V_{RHE}, because the competing $4e^-$ pathway becomes more favorable. In contrast, under illumination, the Ru:CuO/Nb-CBO photocathode achieves an onset potential as low as 1.0 V_{RHE} (**Fig. R4a**). More importantly, it maintains a FE exceeding 90% at both 0.7 and 0.8 V_{RHE} (**Fig. R4b**). This behavior is enabled by the photovoltage generated at the semiconductor/electrolyte interface, which effectively overcomes the thermodynamic limitation that constrains dark electrocatalysts. The photovoltage allows the photocathode to sustain high selectivity for H_2O_2 even at potentials where an electrocatalyst would be less efficient. Thus, the photocathode is therefore essential for achieving self-driven solar H_2O_2 production with high selectivity across a wider potential range.

2) Optical loss from light penetrating the photocathode does not exist in our system. In the lab-scale bias-free test setup, the FTO substrates of the photoanode and photocathode adopt a staggered vertical arrangement, ensuring incident light irradiates both electrodes directly and simultaneously (**Fig. R4c**). For outdoor large-scale tests, the photoanode and photocathode are fixed side by side in the reaction cell, allowing sunlight to irradiate both electrodes unobstructed without the need for "transmitting through one electrode to activate the other," thus completely avoiding optical loss through structural design (**Fig. R4d**). We again thank you for the reviewer's comments.

References

[1] Nie, J., jiang, Q., Sang, Z., Zheng, M., Li, Z., Liu, W., Yang, D., Zheng, Y., Yin, L., Hou, F., Yan, X., Liang, J. Accelerating water dissociation to achieve ampere-level hydrogen peroxide electrosynthesis in brine and seawater. *Nat. Commun*. **16**, 5895 (2025).

[2] Cui, W., Zhen, Z., Sun, Y., Liu, X., Chen, J., Liu, S., Ren, H., Lin, Y., Wu, M., Li, Z. Vacancy-Activated B-Doping for Efficient $2e^-$ Oxygen Reduction through Suppressing H_2O_2 Decomposition at High Overpotential. *Angew. Chem. Int. Ed.* **64**, e202423056 (2025).

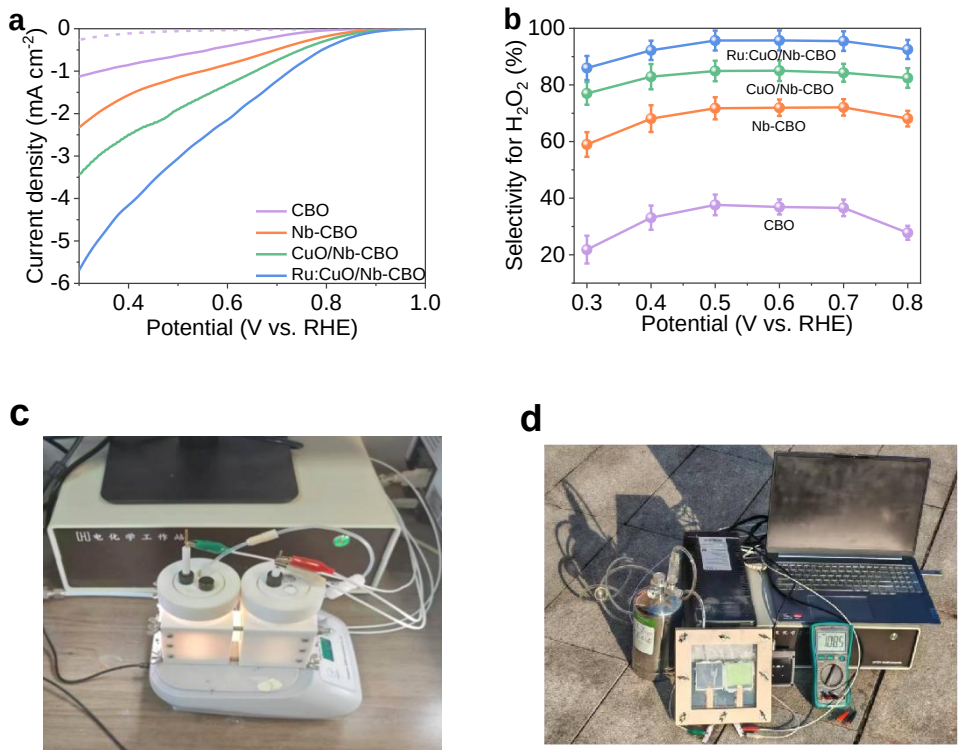

Fig. R4. a, LSV curves of CBO, W-CBO, CuO/Nb-CBO, and Ru:CuO/Nb-CBO under AM 1.5G illumination. **b**, FEs of H_2O_2 at various applied potentials for the corresponding samples. **c**, Photo of the bias-free system. **d**, Digital image of real outdoor solar tests.

9. The manuscript title includes the term “tandem PEC”. However, Figure 4a shows that the cathode and anode are spatially separated. Therefore, the use of the term “tandem PEC” appears to be inappropriate.

Response: Thank you for your insightful comment. We appreciate the opportunity to clarify the rationality of using the term tandem PEC in the manuscript title, which is based on the integral structural design and operational mechanism of our photoelectrochemical system. Specifically, the Ru:CuO/Nb-CBO photocathode and Zn-TiO_2/BVO/WO_3 photoanode are integrated in a single reaction system without any spatial separation, as the schematic in **Fig. R5**. This figure only visually distinguishes their functional regions for clarity in illustrating reaction pathways rather than representing actual physical separation, and both electrodes are immersed in the same 1 M $NaHCO_3$ + 1 M NaOH (pH=10) electrolyte without any exchange membrane or physical barrier. The “tandem” here refers to the band energy level matching and functional synergistic cooperation between the two electrodes, which enables the spontaneous generation of photovoltage to drive the coupled $2e^-$ reactions for H_2O_2 production under light illumination without external electrical bias. Efficient charge

transfer and ion conduction are realized through the shared electrolyte, constituting a complete and integrated unbiased tandem PEC system that conforms to the core definition and structural characteristics of a tandem PEC system. Meanwhile, we remove "tandem" from the title to avoid confusion.

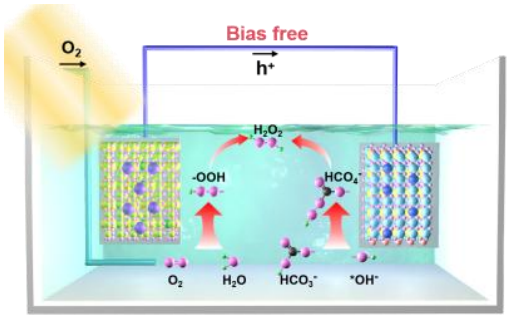

Fig. R5. a Schematic diagram of unbiased tandem device of Ru:CuO/Nb-CBO ‖ Zn-TiO_2/BVO/WO_3 under illumination.

10. Please compare the current density obtained from the 20 cm^2 electrode with that from lab-scale electrochemical measurements under 1 sun illumination. In addition, when scaling up to a large-area electrode, the authors should evaluate and report the electrode uniformity, for example by providing SEM images and XRD data from the corner, edge, and center regions.

Response: Thank you for your valuable comment. We provide the comparative analysis of current density between large-area and lab-scale electrodes, as well as the uniformity evaluation of the scaled-up electrode (**Fig. R6**). Regarding the current density comparison: the illumination intensity of outdoor natural sunlight tests did not reach the standard 1 sun (100 mW cm^{-2}), so we conducted comparative tests under simulated 0.73 sun illumination (73 mW cm^{-2}) to ensure consistent test conditions. Ideally, the total current of a 36 cm^2 electrode should be 36 times that of a 1 cm^2 lab-scale electrode if the current density remains unchanged. However, our experimental results show that the total current of the 36 cm^2 electrode is only about 26 times that of the 1 cm^2 electrode. This discrepancy is mainly attributed to increased series resistance from the larger electrode area and greater mass-transport limitations (e.g., O_2 and HCO_3^- diffusion) in the larger cell, all of which cause a decrease in the effective current density upon scale-up. We collected samples from three typical regions (corner, edge, and center) for XRD and SEM characterizations. XRD patterns of all regions exhibit identical diffraction peaks corresponding to Zn-TiO_2/BVO/WO_3 photoanode and Ru:CuO/Nb-CBO

photocathode without obvious peak shifts or intensity variations, confirming consistent crystal structure. SEM images reveal uniform nanoworm-like morphology for Zn-TiO_2/BVO/WO_3 and nanosheet morphology for Ru:CuO/Nb-CBO across all regions, with no significant differences in thickness or particle distribution. These results fully verify the excellent uniformity of the large-area electrode.

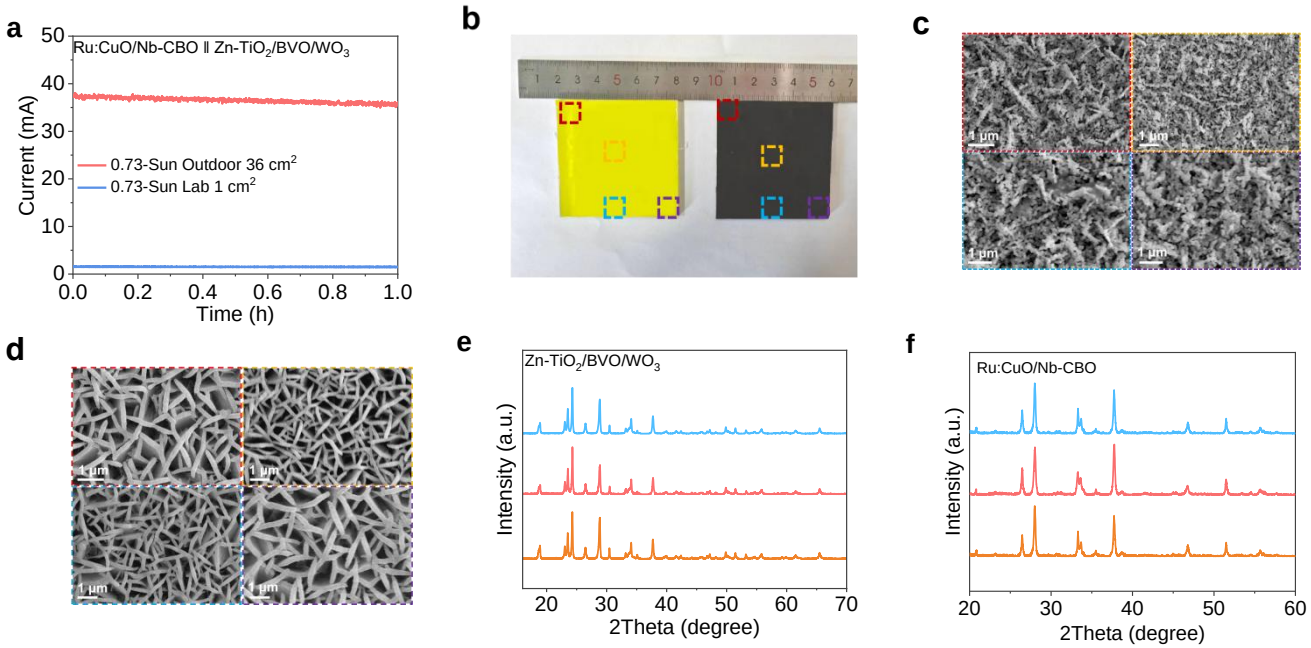

Fig. R6. a I-t curves of Ru:CuO/Nb-CBO ‖ Zn-TiO_2/BVO/WO_3 cell under real sun (36 cm^2 for both photoelectrodes) and simulated sunlight illumination (1 cm^2 for both photoelectrodes). **b** Images of the photoelectrode. **c**, **d** SEM images of all regions to **c** Zn-TiO_2/BVO/WO_3 and **d** Ru:CuO/Nb-CBO. **e**, **f** XRD patterns of all regions to **e** Zn-TiO_2/BVO/WO_3 and **f** Ru:CuO/Nb-CBO.

11. Although a 20 cm^2 electrode is described as a large-area system, this scale is still relatively small for meaningful scale-up demonstrations. The authors are encouraged to further increase the electrode size.

Response: Thank you for your constructive comment. We have optimized the preparation process to fabricate 36 cm^2 (6×6 cm) dual photoelectrodes (Zn-TiO_2/BVO/WO_3 photoanode and Ru:CuO/Nb-CBO photocathode).

The 36 cm^2 large-area electrodes were prepared via a modified scalable fabrication strategy, including uniform large-area hydrothermal growth for WO_3 nanosheets, controlled electrodeposition for $BiVO_4$ and $CuBi_2O_4$ layers, and atomic layer deposition for the conformal TiO_2 passivation layer,

which ensures excellent structural and morphological uniformity across the entire electrode surface. Performance tests under natural sunlight show that the 36 cm^2 tandem PEC system maintains a stable initial photocurrent density of 36 mA, with a total H_2O_2 FE of 164.3% and a yield of 11.44 mmol L^{-1} during 1 h continuous operation.

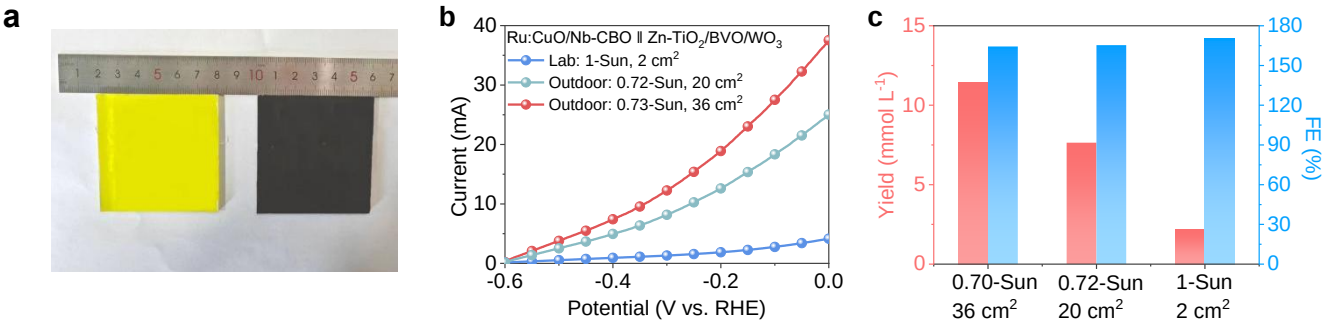

Fig. R7. a Images of the photoelectrode. **b** *J-V* curves of Ru:CuO/Nb-CBO || Zn-TiO_2/BVO/WO_3 cell under real sun (36 and 20 cm^2 for both photoelectrodes) and simulated sunlight illumination (2 cm^2 for both photoelectrodes). **c** Corresponding H_2O_2 FEs and yields for 1 h test.

12. Please provide photographs of the actual experimental setup. Moreover, the experimental details should be described more explicitly, including parameters such as the solution volume of the cathode and anode.

Response: We appreciate the reviewer's professional comment. We provide comprehensive experimental details, supported by actual photographs, to address light management, glycerol solubility maintenance, and concentration control as follows.

1) Laboratory setup. In the laboratory, the unbiased tandem PEC measurements were conducted in a two-compartment H-type cell separated by a Nafion 117 proton exchange membrane (effective area 1 cm^2) (**Fig. R8**). Each compartment contained 30 mL of electrolyte (1 M $NaHCO_3$, pH=10). The photoanode (Zn-TiO_2/BVO/WO_3) and photocathode (Ru:CuO/Nb-CBO), each with an active area of 1 cm^2 or 2 cm^2, were immersed in their respective compartments. Illumination was provided by a solar simulator (AM 1.5G, 100 mW cm^{-2}) from the photoanode side.

2) Outdoor test setup. For natural sunlight validation, a custom-built single-compartment PEC reactor was used. The reactor had a total electrolyte volume of 100 mL. Both the photoanode and photocathode (each 20 cm^2) were immersed in the same electrolyte without a membrane, as the system operates under bias-free conditions, and both electrodes produce H_2O_2 in the same solution. The

reactor was placed under direct natural sunlight, and solar irradiance was recorded during the tests.

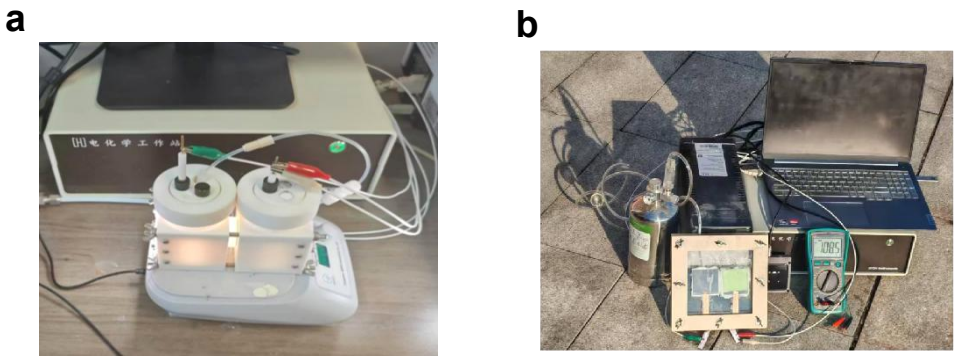

Fig. R8. a Photo of the bias-free system. **b** Digital image of real outdoor solar tests.

13. The in-situ ATR-SEIRAS results support the authors' claims well. However, this analysis does not provide information on where OOH is formed on the surface. If available, in-situ XANES or EXAFS results would allow more definitive identification of the active sites. If such analyses are challenging, are there alternative approaches to clearly verify that Zn, Ti, and Ru are the active sites?

Response: We appreciate the reviewer's valuable questions. We employ selective active site poisoning experiments combined with open circuit potential (OCP) tests to identify the formation sites of *OOH intermediates and verify that Zn, Ti, and Ru serve as the active sites for H_2O_2 synthesis. The OCP test reflects the interfacial electronic structure changes of the electrode surface induced by the adsorption and activation of reaction intermediates; a distinct OCP variation indicates the direct participation of the targeted active sites in the catalytic reaction.

1) For the Zn-TiO_2/BVO/WO_3 photoanode, we used F^- to poison Ti active sites by forming stable Ti-F bonds, and CN^- to poison Zn active sites by forming inert Zn-CN complexes.[1,2] Under 2e^- WOR conditions, the unpoisoned photoanode showed almost no OCP variation (**Fig. R9a**). In contrast, both the F^--poisoned (Ti poisoned) and CN^--poisoned (Zn poisoned) samples exhibited a significant negative OCP shift, indicating that poisoning of the active sites disrupts the adsorption/activation of reaction intermediates. The FE for H_2O_2 followed a clear trend (**Fig. R9c**): the unpoisoned photoanode achieved an FE of 90.2%. Poisoning Ti with F^- reduced the FE to 35.9%, poisoning Zn with CN^- reduced the FE to 65.8%, and simultaneous poisoning of both Ti and Zn drastically lowered the FE to 7.4%. These results demonstrate that both Zn and Ti are active sites for *OOH intermediate formation and anodic H_2O_2 generation, with Ti playing a more dominant role.

2) For the Ru:CuO/Nb-CBO photocathode, we used S^{2-} to poison Ru active sites by forming inert RuS_2. Under $2e^-$ ORR conditions, the unpoisoned photocathode exhibited almost no OCP change, whereas the S^{2-}-poisoned sample showed a significant positive OCP shift (**Fig. R9b**). Correspondingly, the H_2O_2 FE of the poisoned photocathode dropped dramatically from 91.9% to 13.4% (**Fig. R9d**), directly confirming that Ru is the key active site for *OOH intermediate stabilization and cathodic H_2O_2 synthesis.

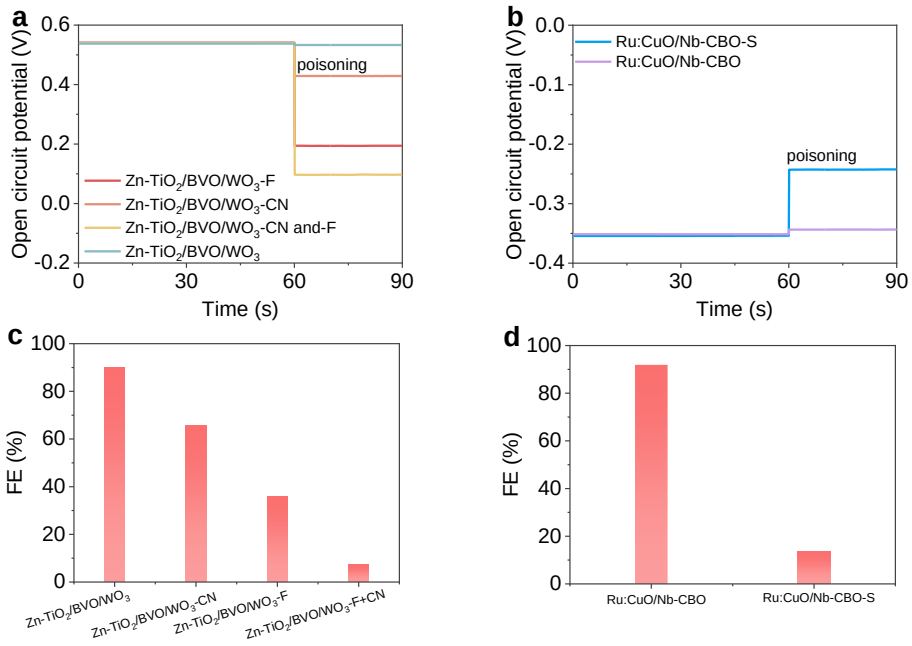

Fig. R9. a, b OCPs of **a** Zn-TiO_2/BVO/WO_3 and **b** Ru:CuO/Nb-CBO in 1 M $NaHCO_3$ (pH=10) before and after poisoning. **c, d** FEs of **c** Zn-TiO_2/BVO/WO_3 and **d** Ru:CuO/Nb-CBO in 1 M $NaHCO_3$ (pH=10) before and after poisoning.

References

[1] Zhou, P., Lv, X., Tao, S., Wu, J., Wang, H., Wei, X., Wang, T., Zhou, B., Lu, Y., Fraueheim, T., Fu, X., Wang, S., Zou, Y. Heterogeneous-Interface-Enhanced Adsorption of Organic and Hydroxyl for Biomass Electrooxidation. *Adv. Mater.* **34**, 2204089 (2022).

[2] Luo, W., Tian, H., Li, Q., Ma, J., Sun, W., Zhu, L., Wu, H., Kong, F., Zhuang, X., Cui, X., Shi, J. Controlled Electrocatalytic Glycerol Upgrading to Glyceraldehyde in Near Neutral Media by Cobalt Oxide Lattice Activation. *Angew. Chem. Int. Ed.* **64**, e202505059 (2025).

Reviewer #3:

We thank the reviewer 3 for the positive comments of our manuscript. We have made the suggested revision.

In this manuscript, the authors report a bias-free tandem photoelectrochemical (PEC) system for hydrogen peroxide (H_2O_2) production by integrating two-electron water oxidation ($2e^-$ WOR) at a Zn–TiO_2/$BiVO_4$/WO_3 photoanode with two-electron oxygen reduction ($2e^-$ ORR) at a Ru:CuO/Nb–CBO photocathode. The study demonstrates relatively high Faradaic efficiencies for both half-reactions, operation in an unassisted configuration, outdoor validation under natural sunlight, and bacterial inactivation tests. The manuscript is supported by extensive experimental characterization, in situ spectroscopy, and DFT calculations. The work presents several strengths, particularly the integration of both half-reactions in a bias-free system and the breadth of mechanistic analysis. However, significant concerns remain regarding mechanistic clarity, interpretation of Faradaic efficiency values (especially total FE >100%), justification of material selection, and benchmarking against prior literature. In its current form, the conceptual rigor and critical analysis do not reach the level expected for publication in Nature Communications.

1. Insufficient mechanistic clarity regarding the role of Zn, Nb, and Ru. Although the authors attribute performance enhancement to heterojunction engineering and dopant effects, the mechanistic explanation remains largely qualitative and insufficiently substantiated. The specific role of Zn incorporation in TiO_2 is not convincingly demonstrated. Is Zn acting as a shallow donor, modifying surface adsorption energetics, altering band bending, or passivating surface recombination sites? The evidence provided (minor XPS shifts, d-band center modulation in DFT) is indirect and does not clearly establish causal relationships with selectivity enhancement. Similarly, the rationale for choosing Nb doping in CBO and Ru decoration on CuO/Nb–CBO lacks systematic justification. Why were these particular dopants selected over alternatives? Are there control experiments comparing different dopants or loadings? The selectivity improvement is primarily explained by reduced impedance and increased electrochemical surface area. However, selectivity in multi-electron electrochemical reactions is governed by reaction pathway energetics and intermediate binding thermodynamics, not simply by reduced charge-transfer resistance or larger surface area. The current

discussion does not sufficiently bridge kinetic observations with intrinsic catalytic selectivity. A more rigorous structure–property–performance correlation is required to support the mechanistic claims.

Response: Thank you for your insightful and professional comments. We have thoroughly revised the relevant mechanistic sections, supplemented systematic experimental characterizations and in-depth theoretical calculations, and added control experiments for dopant selection and loading optimization.

1. **Specific role of Zn in TiO_2: from shallow donor to surface adsorption and band bending modulation**

1) **Shallow donor and conductivity enhancement:** DFT calculations of the density of states (DOS) show that Zn introduces impurity energy levels of TiO_2 (shallow donor levels), increasing the free electron concentration. This is experimentally supported by a higher charge transport rate constant (k_{trans}) from IMPS and lower charge-transfer resistance from EIS for Zn-TiO_2/BVO/WO_3 compared to undoped TiO_2/BVO/WO_3 (**Fig. R1a-c**).

2) **Enhance charge separation efficiency:** Steady state photoluminescence (PL) and time resolved PL (TRPL) measurements (**Fig. R1d and e**) reveal that Zn doping reduces the PL emission intensity and prolongs the average carrier lifetime from 0.87 ns (TiO_2/BVO/WO_3) to 0.88 ns (Zn-TiO_2/BVO/WO_3). This extended lifetime of Zn-TiO_2/BVO/WO_3 confirms that Zn doping and type-II heterojunction engineering synergistically suppress charge recombination and enhance charge separation efficiency.

3) **Modification of surface adsorption energetics:** This upward shift strengthens the interaction with $*HCO_3^-$, leading to a more favorable ΔG for the $*HCO_4^-$ intermediate (-0.17 eV) compared to TiO_2/BVO/WO_3 (+0.31 eV) and BVO/WO_3 (+0.46 eV). At the same time, the ΔG for the *OOH intermediate in the $4e^-$ OER increases from +0.47 eV (TiO_2/BVO/WO_3) to +0.49 eV (Zn-TiO_2/BVO/WO_3) (**Fig. 6b and 6c**). The clear size relationship - lower ΔG for the $2e^-$ pathway and higher ΔG for the $4e^-$ pathway - directly explains the observed FE increase from 74% for TiO_2/BVO/WO_3 to 90.2% for Zn-TiO_2/BVO/WO_3 at 0.6 V_{RHE} (**Fig. 2b**).

4) **Alteration of interfacial band bending:** Ultraviolet photoelectron spectroscopy (UPS) measurements (**Fig. R1f-h**) show that Zn doping induces a positive shift of the Fermi level of TiO_2, which enhances the built in electric field at the TiO_2/BVO interface. This is further evidenced by the increased positive shift of Bi 4*f* and V 2*p* XPS core levels (**Figs. 1h and S4a**), indicating more efficient electron extraction from $BiVO_4$. A stronger band bending facilitates hole migration to the surface,

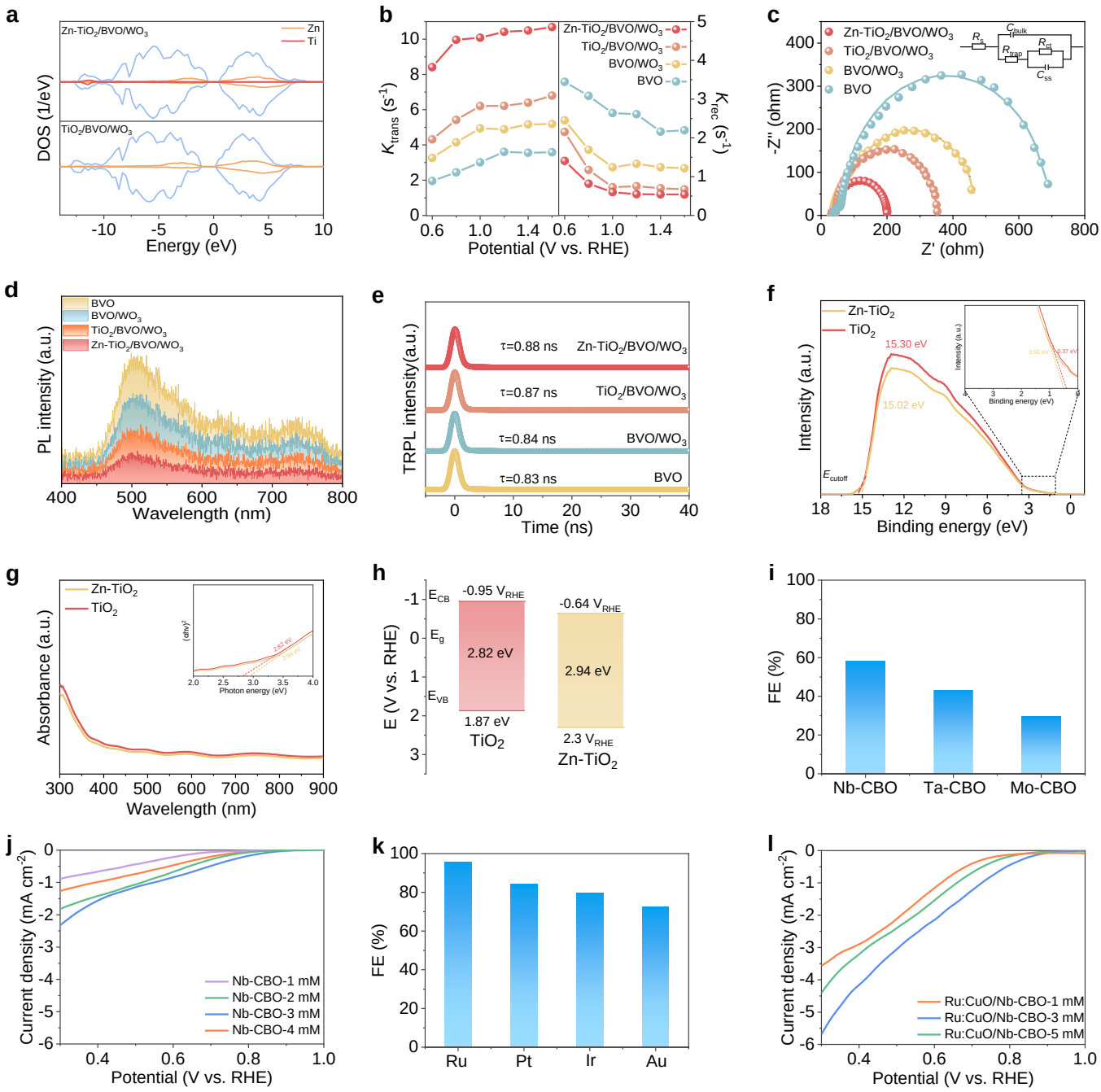

Fig. R1. a DOS of surface states for TiO_2/BVO/WO_3 and Zn-TiO_2/BVO/WO_3. **b** Charge transfer (k_{trans}) and charge recombination (k_{rec}) rate constants from IMPS spectra. **c** EIS, **d** PL, and **e** TRPL decay spectra for corresponding photoanodes. Inset of **c** shows the corresponding circuit model. **f** UPS spectra of TiO_2 and Zn-TiO_2. Inset shows the zoomed-in image area in the black dashed lines. **g** UV-vis spectra of TiO_2 and Zn-TiO_2. Inset shows the optical band gaps. **h** Band alignments of TiO_2, and Zn-TiO_2. **i** FEs of CBO with different dopant elements. **j** LSV curves of Nb-CBO with various concentrations of niobamyl oxalate. **k** FEs of CuO/Nb-CBO with different dopant elements. **l** LSV curves of Ru:CuO/Nb-CBO with various contents of $Ru(acac)_2$.

reducing bulk recombination and improving selectivity.

Collectively, these data demonstrate that Zn acts as a shallow donor, passivates recombination sites, modifies intermediate adsorption energetics, and modulates band bending. All of which synergistically contribute to the enhanced $2e^-$ WOR selectivity.

2. **Rationale for Nb doping in $CuBi_2O_4$ (CBO) and control experiments.**

Nb was selected as the dopant for CBO because: (i) Nb^{5+} has a similar ionic radius to Bi^{3+} and Cu^{2+}, allowing lattice incorporation without major structural distortion. (ii) Nb is a common n-type dopant for p-type semiconductors, increasing donor density and improving charge transport. (iii) preliminary screening of alternative dopants (Ta, Mo) at the same nominal concentration (3 mM) showed that Nb gave the highest H_2O_2 FE (57.98%) compared to Ta (43.27%) and Mo (29.51%) at 0.6 V_{RHE} (**Fig. R1i**). The optimal Nb loading was determined by varying the concentration (1, 2, 3, and 4 mM). The 3 mM gave the best balance between conductivity and active site exposure (**Fig. R1j**).

3. **Rationale for Ru decoration on CuO/Nb-CBO and alternative cocatalyst comparison.**

Ru nanoparticles were chosen because: (i) Ru is known to facilitate the protonation of $*OO^-$ to *OOH, a key step in the $2e^-$ ORR. (ii) control experiments with other noble metals (Pt, Au, Ir) deposited under identical conditions showed that Ru gave the highest H_2O_2 FE (95.7%), followed by Pt (84.2%), Ir (79.5%), and Au (72.3%) (**Fig. R1k**). The optimal Ru loading was determined by varying the concentration of $Ru(acac)_2$ (1, 3, and 5 mM), in which 1 mM gave the best performance (**Fig. R1l**). The related information has been added in Supporting Information of **Supplementary Figs. 40 and 41.**

4. **Distinguishing activity from selectivity: bridging kinetics and thermodynamics.**

We agree with the reviewer that reduced impedance and increased ECSA explain improved activity (higher photocurrent) but not selectivity. In the revised manuscript, we have explicitly separated these two aspects: (i) Activity is discussed in terms of ECSA, charge-transfer resistance (EIS), and charge transport/recombination constants (IMPS). (ii) Selectivity is discussed exclusively on the basis of intermediate binding free energies (DFT) and in situ spectroscopy (ATR-SEIRAS and Raman).

2. Interpretation of Faradaic efficiency exceeding 100% requires careful reconsideration. The reported total Faradaic efficiency (FE) exceeding 170% in the unassisted system is conceptually problematic

and requires substantially more rigorous explanation. Reporting ~90% FE at both anode and cathode does not justify summing them to claim a "total FE" of ~170%. Faradaic efficiency is defined with respect to the charge passed in a given electrode process. Simply adding individual FEs risks double counting charge and may reflect misunderstanding of electron accounting in a closed circuit. The manuscript does not clearly define how "total FE" is calculated in the unbiased configuration, nor does it provide a strict electron balance analysis. If the anode and cathode each produce H_2O_2 independently in separated compartments, the correct interpretation should be clarified in terms of charge conservation and net reaction stoichiometry. Because FE >100% contradicts fundamental electrochemical definitions unless carefully defined, this issue must be resolved rigorously. As it stands, it raises concerns about the validity of the quantitative analysis.

Response: Thank you for this extremely rigorous and critical comment on the definition and interpretation of FE. We agree that the previous description of "total FE > 170%" lacked a strict electrochemical definition and clear electron-balance analysis, which could lead to misunderstanding of charge accounting in a closed circuit. We sincerely apologize for this conceptual ambiguity and have completely revised the relevant definitions, calculation methods, and narrative expressions in the manuscript, accompanied by a strict electron conservation verification.

1) **Two-compartment H-cell with proton exchange membrane (PEM).** In the laboratory two-compartment H-cell separated by a Nafion PEM (**Fig. 4b-e**), the anolyte and catholyte are physically isolated. The photoanode (Zn-TiO_2/BVO/WO_3) catalyzes the $2e^-$ water oxidation reaction (WOR) to produce H_2O_2, and the photocathode (Ru:CuO/Nb-CBO) catalyzes the $2e^-$ oxygen reduction reaction (ORR) to produce H_2O_2. Because the two compartments are separated, the charge passing through the external circuit (Q_{total}) is the same for both electrodes ($Q_{total} = Q_{anode} = Q_{cathode}$). However, each electrode's FE is defined independently against its own half-reaction charge, and the theoretical maximum FE for a single electrode is 100%.[1,2] In our H-cell measurements, the photoanode achieved an FE of ~90% and the photocathode achieved an FE of ~92%, both well within the 100% limit.

2) **Unassisted outdoor single-compartment cell (no membrane) (Fig. R2a).** In the outdoor tests under natural sunlight, the tandem cell was operated in a **single-compartment (PEM-free) configuration** (**Fig. 4f and 4g**). Here, both electrodes are immersed in the same electrolyte without any physical separation. The same photogenerated electrons that flow from the photoanode to the photocathode through the external circuit drive both half-reactions simultaneously. Specifically:

Anode ($2e^-$ WOR): $2H_2O \rightarrow H_2O_2 + 2H^+ + 2e^-$

Cathode ($2e^-$ ORR): $O_2 + 2H^+ + 2e^- \rightarrow H_2O_2$

For each electron that passes through the external circuit, one H_2O_2 molecule is produced at the cathode (via $2e^-$ ORR) and one H_2O_2 molecule is enabled at the anode (via $2e^-$ WOR, using the photogenerated hole). Therefore, when both half-reactions operate at 100% FE, the combined H_2O_2 yield per electron reaches 200% (one H_2O_2 from each electrode per electron).[3,4] This is not a violation of charge conservation but rather a direct consequence of the matched $2e^-$ tandem design in a shared electrolyte. For the unbiased single-compartment system, we define the combined H_2O_2 yield per electron (or system-level "total FE") as:

$$\text{Total FE} = \frac{2F(n_{anode}+n_{cathode})}{Q_{total}} \times 100\%$$

where n_{anode} and $n_{cathode}$ are the amounts of H_2O_2 produced at the photoanode and photocathode, respectively, and Q_{total} is the total charge recorded by the external circuit. This definition avoids double-counting charge and strictly adheres to charge conservation, because Q_{total} represents the only charge loop driving both half-reactions simultaneously. The individual FE of each electrode, when calculated against its own half-reaction charge, remains ≤100% (e.g., ~90% for the anode and ~92% for the cathode). The combined value of ~170% simply reflects that the same charge produces H_2O_2 at both electrodes.

3) We provide strict electron-balance verification to validate the rationality of the total FE value. We calculated the total theoretical electron consumption $2F(n_{anode}+n_{cathode})$ from measured H_2O_2 yields and compared it with the experimentally recorded Q_{total}. The relative error between the calculated electron amount and the measured circuit charge is < 3%, confirming strict charge conservation in the system. The total FE of ~170% arises because both electrodes convert the same loop charge into the target $2e^-$ product, rather than any violation of electrochemical fundamentals. In addition, the validity of total FE > 100% in a membrane-free configuration is supported by previous literatures, including ***Nat. Catal.* 2020, 3, 125** reported by Haotian Wang et al., ***Nat. Commun.* 2023, 14, 5822** reported by Liming Dai et al., and ***Adv. Funct. Mater.* 2025, 35, 2425301** reported by Yongmei Chen et al., which explicitly describe that two H_2O_2 molecules can be generated per electron loop when both $2e^-$ half-reactions operate concurrently (**Fig. R2b-d**).[5-7] These references are now cited in the revised manuscript. Moreover, we remove the word (170%) in the title to avoid misunderstanding.

We are willing to further discussion if having any unclear part.

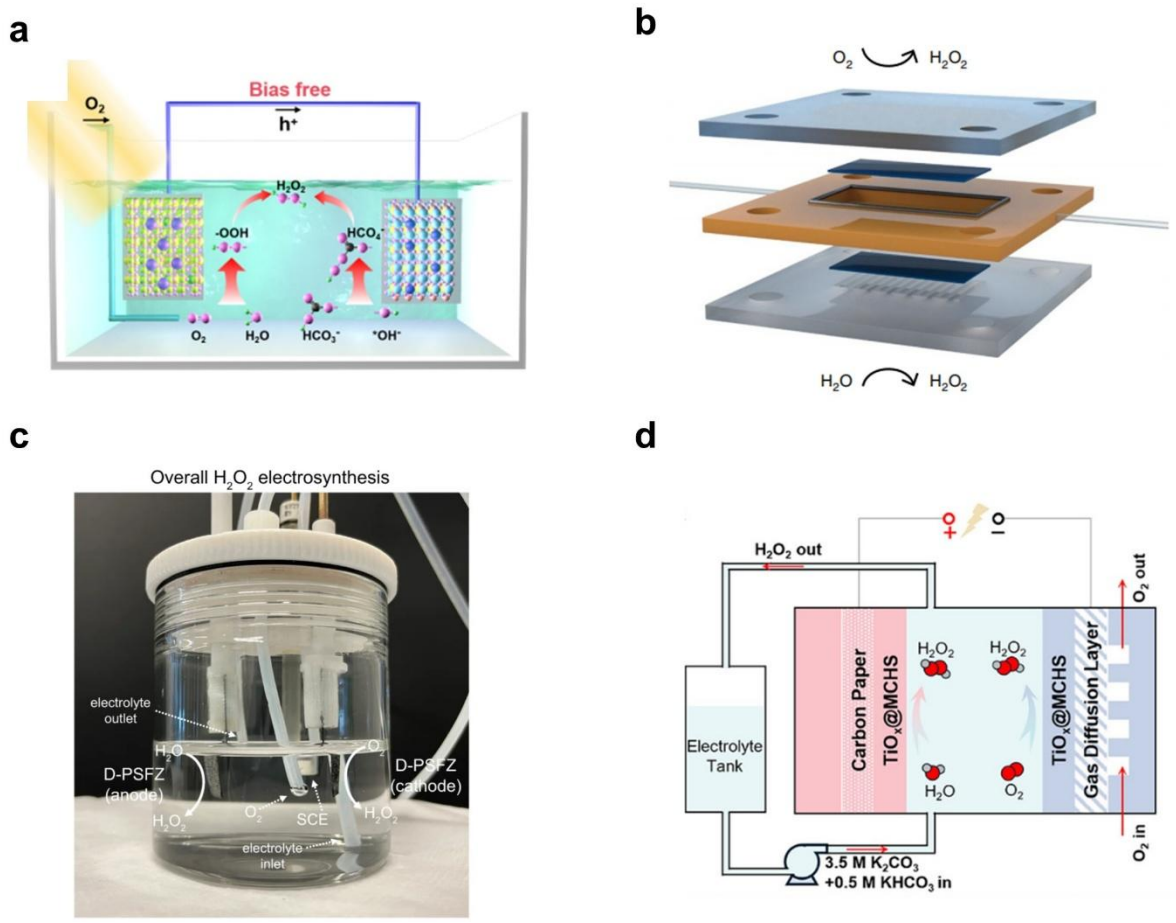

Fig. R2. a Schematic diagram of unbiased tandem device of Ru:CuO/Nb-CBO ‖ Zn-TiO_2/BVO/WO_3 under illumination. **b** Schematic design of our H_2O_2 production protype cell.[5] **c** Photograph of the membrane-free overall H_2O_2 electrosynthesis unit in a three-electrode configuration using the D-PSFZ as both cathode and anode (denoted as D-PSFZ||D-PSFZ) with a SCE reference electrode.[6] **d** The schematic diagram of the composition of the 2e-WOR//2e-ORR cell.[7]

References

[1] Jeon, T. H., Kim, H., Kim, H., Choi, W. Highly durable photoelectrochemical H_2O_2 production via dual photoanode and cathode processes under solar simulating and external bias-free conditions. *Energy Environ. Sci.* **13**, 1730 (2020).

[2] Jeon, T. H., Koo, M. S., Kim, H., Choi, W. Dual-Functional Photocatalytic and Photoelectrocatalytic Systems for Energy- and Resource-Recovering Water Treatment**.** *ACS Catal.* **8**, 11542-11563 (2018).

[3] Wang, Z., Li, K., Hu, J., Li, A., Tang, Y., Sun, Y., Wan, P., Jiang, H., Chen, Y. Dual-Functional Catalyst of Amorphous TiO_2 Embedded in Mesoporous Carbon Hollow Spheres for H_2O_2 Electrosynthesis. *Adv. Funct. Mater.*

35, 2425301 (2025).

[4] Yan, M., Yang, H., Gong, Z., Zhu, J., Allen, C., Cheng, T., Fei, H. Sulfur-Tuned Main-Group Sb−N−C Catalysts for Selective 2-Electron and 4-Electron Oxygen Reduction. *Adv. Mater.* **36**, 2402963 (2024).

[5] Xia, C., Back, S., Ringe, S., Jiang, K., Chen, F., Sun, X., Siahrostami, S., Chan, K., Wang, H. Confined local oxygen gas promotes electrochemical water oxidation to hydrogen peroxide. *Nat. Catal*. **3**, 125 (2020).

[6] Kim, C., Park, S. O., Kwak, S. K., Xia, Z., Kim, G., Dai, L. Concurrent oxygen reduction and water oxidation at high ionic strength for scalable electrosynthesis of hydrogen peroxide. *Nat. Commun*. **14**, 5822 (2023).

[7] Wang, Z., Li, K., Hu, J., Li, A., Tang, Y., Sun, Y., Wan, P., Jiang, H., Chen, Y. Dual-Functional Catalyst of Amorphous TiO_2 Embedded in Mesoporous Carbon Hollow Spheres for H_2O_2 Electrosynthesis. *Adv. Funct. Mater.* **35**, 2425301 (2025).

3. Benchmarking and literature comparison are not sufficiently fair or comprehensive. The manuscript compares its performance with selected prior reports; however: There are published studies reporting higher half-reaction Faradaic efficiencies for both $2e^-$ WOR and $2e^-$ ORR individually. These are not adequately discussed. The comparison does not consistently normalize parameters such as illumination intensity, electrolyte composition, applied bias, electrode area, or measurement duration. Claiming "highest FE" without comprehensive benchmarking may be misleading. A more balanced and quantitative comparison table, including half-cell and full-cell systems under equivalent conditions, is necessary to substantiate claims of advancement.

Response: Thank you for your insightful and critical comment. We have thoroughly revised the literature comparison part of the manuscript, with systematic supplements and improvements as follows:

(1) We have expanded the literature scope to include published studies that report higher FEs for individual $2e^-$ WOR and $2e^-$ ORR half-reactions, and added an objective and in-depth discussion of their performance characteristics and experimental conditions (**Tables R1 and R2**). Our work focuses on bias-free tandem PEC systems with integrated $2e^-$ WOR and $2e^-$ ORR, and realizes high FE under large-area electrode (20 cm^2), long-term stable operation (>10 h) and a single compatible electrolyte (1 M $NaHCO_3$ + 1 M NaOH, pH=10). We objectively acknowledge the advantages of those high-FE half-reaction studies, and meanwhile highlight the unique advancement of our work in the integration, practicality and stability of the full tandem system, which is the core research focus of this manuscript.

(2) We have constructed a quantitative and balanced comparison table specifically focusing on bipolar H_2O_2 production systems. We have strictly normalized all key comparison parameters including electrolyte composition and pH, applied bias, measurement duration, FE and other core performance metrics. The table is categorized by test conditions for clear classification. All cited studies are rigorously normalized to ensure fair and comparable benchmarking. We focus exclusively on bipolar systems for H_2O_2 synthesis. We compare our work with the latest reported bipolar H_2O_2 production systems in terms of comprehensive performance. We also explicitly mark the differences in experimental conditions between each referenced study and our work to enhance the rigor and targeting of the comparison (**Table R3**).

(3) We have revised the relevant performance claims in the manuscript. We clearly state the performance advantages of our work under specific practical conditions. Our unassisted tandem PEC system maintains a FE of 163.37% with a 36 cm^2 large-area electrode under natural sunlight in a membrane-free configuration, demonstrating its practical scalability without the need for proton exchange membranes. Importantly, as explicitly described in Haotian Wang et al.'s work in **Nat. Catal. 2020, 3, 125**, Liming Dai et al.'s work in **Nat. Commun. 2023, 14, 5822**, and Yongmei Chen et al.'s work in **Adv. Funct. Mater. 2025, 35, 2425301**, a total FE exceeding 100% is feasible in membrane-free configurations because the two electrons shuttling from the anode to the cathode can be fully utilized to generate two H_2O_2 molecules, one at each electrode.[1-3]

Table R1 Summary of PEC WOR H_2O_2 performance of recently reported photoanodes under AM 1.5G illumination.

Sample	Electrolyte	η_{H2O2} (μmol cm^{-2} min^{-1})	FE (1.23 V_{RHE})	J (1.23 V_{RHE}) (mA cm^{-2})	Stability	Reference
Zn-TiO_2/BVO/WO_3	**1 M $NaHCO_3$ (pH=10)**	**1.469 (1.23 V_{RHE})**	**90.2%**	**5.07**	**10 h**	**This work.**
CPF-CzPB/Mo:$BiVO_4$	1 M $KHCO_3$ (pH=9)	1.23 (1.23 V_{RHE})	94.08%	4.3	120 h	Adv. Mater.2025, 37, e08326
SnO_{2-x}/$BiVO_4$	1 M $NaHCO_3$ (pH=8.3)	0.825 (1.23 V_{RHE})	88%	~3.8	1 h	J.Am. Chem. Soc. 2020, 142, 8641.
P-Mo-$BiVO_4$	1 M $NaHCO_3$ (pH=8.3)	0.21 (1.0 V_{RHE})	46%	~1.8	5 h	Energy Environ. Sci.2020, 13, 1730.
$BiVO_4$/Au-PAT	1 M $NaHCO_3$ (pH=8.3)	0.312 (1.23 V_{RHE})	72.10%	~1.66	2 h	ACS Energy Lett. 2023, 8, 5192.

$CaSnO_3/SrTiO_3/BiVO_4$	1 M $NaHCO_3$ (pH=8.3)	0.825 (1.2 V_{RHE})	90%	~2.99	3 h	ACS Energy Lett. 2024, 9, 1415.
N-O_{vac}-$BiVO_4$-350	1 M $NaHCO_3$ (pH=8.3)	~0.76 (1.6 V_{RHE})	81.20%	~2.9	2 h	ACS Energy Lett. 2022, 7, 3024.
O-$BiVO_4$	2 M $KHCO_3$	---	42.80%	~0.5	---	ACS Catal. 2024, 14, 5297.
$Ni_5P_4/NiO/BiVO_4$	2 M $KHCO_3$	0.313 (1.2 V_{RHE})	76.5%	4.05 (1.78 V_{RHE})	---	Chem. Eng. J. 2025, 510, 161667.
$ZnO/BiVO_4$	2 M $KHCO_3$	---	31.60%	2.83	10 min	J. Energy Chem. 2025, 103, 877.
Co_3O_4@Pt-Fe_2O_3	2 M $KHCO_3$	0.073	77.38%	1.35	---	Chem. Eng. J. 2023, 473, 145384.
$ZnIn_2S_4$-Se/QDs	1 M $NaHCO_3$ (pH=8.3)	---	86%	4.2	7 h	Chem. Eng. J. 2024, 491, 151925.
A-TP/TiO_2	1 M $KHCO_3$ (pH=9)	0.225 (1.76 V_{RHE})	63%	0.46 (1.76 V_{RHE})	---	J. Energy Chem. 2023, 86, 399.

Table R2. Summary of PEC ORR H_2O_2 performance of recently reported photocathodes under AM 1.5G illumination.

Sample	Electrolyte	Stability	FE (0.6 V_{RHE})	Onset potential (V_{RHE})	Reference
Ru:CuO/W-CBO	**1 M $NaHCO_3$ (pH=10)**	**50 h**	**91.93%**	**1.0**	**This work.**
CPF-CzAD	1 M $KHCO_3$ (pH=9)	120 h	90.8 %	---	Adv. Mater. 2025, 37, e08326.
O-BP/FM-PSK	0.1 M KOH	12 h	100%	0.85	Nat. Commun. 2021, **12**, 6644.
$Cu_3BiS_3/CdS/TiO_2/MoO_x/Mo$	0.2 M KOH	14 h	100%	0.9	Energy Environ. Sci. 2024, **17**, 5588.
$Au/CuBi_2O_4/PtSe_2$	0.1 M $KHCO_3$	3 h	35%	1.0	Adv. Funct. Mater. 2023, **33**, 2303391.
$Na_2Co_2O_4/CuBi_2O_4$	0.1 M $KHCO_3$ with 0.1 M $Na_2S_2O_8$	1 h	47.42%	1.0	App. Catal. B 2022, **304**, 120980.
Au-In_2S_3/Cu_3BiS_3	0.1 M PBS	2 h	71%	0.5	Appl. Catal. B 2022, **307**, 121152.
O-BP/FM-PSK	0.1 M KOH	12 h	100%	0.85	Nat. Commun. 2021, **12**, 6644.

Table R3. Summary of bipolar H_2O_2 performance of recently reported.

System	Sample	Applied bias (V_{RHE})	η_{H2O2} (μmol cm^{-2} min^{-1})	FE	Stability	Current density (mA cm^{-2})	Reference
PEC ‖ PEC	**Zn-TiO_2/BVO/WO_3‖ Ru:CuO/Nb-CBO ‖**	**unbiased**	**1.07**	**Total:163.37%**	**10 h**	**2.1**	**This work.**
PEC ‖ PEC	CPF-CzPB/Mo:$BiVO_4$ ‖ CPF-CzAD	unbiased	1.083	---	~168 h	1.85	Adv. Mater.2025, 37, e08326
PEC ‖ PEC	$CaSnO_3$/SnO_2/$BiVO_4$ ‖ PV	unbiased	---	Photoanode:90%	5 h	5.77	Adv. Energy Mater 2026, 16, e05447.
PEC ‖ EC	RuOx/TNR‖AQ-graphite	unbiased	---	Total:90%	100 h	1.23	Energy Environ. Sci. 2021, 14, 3110.
PEC ‖ EC	P-Mo-BVO ‖ AQ-CNT/C	unbiased	0.16	Photoanode:43% Cathode:100%	5 h	---	Energy Environ. Sci. 2020, 13, 1730.
EC ‖ EC	O-CNTs ‖ PTFE-C	1.7	24	Total:153%	~3 h	120	Nat. Catal. 2020, 3, 125.
EC ‖ EC	D-PSFZ ‖ D-PSFZ	2.1	---	Total:163%	100 h	50	Nat. Commun. 2023, 14, 5822.

4. Overemphasis on impedance and ECSA as explanations for selectivity. Throughout the manuscript, performance improvements are frequently attributed to: Reduced charge-transfer resistance (EIS), Higher ktrans and lower krec (IMPS), Increased electrochemical surface area (ECSA). While these factors explain improved activity or stability, they do not inherently explain improved reaction selectivity between $2e^-$ and $4e^-$ pathways. Selectivity depends on relative free energy barriers of competing intermediates and their surface coverage dynamics. Although DFT calculations are presented, the discussion remains descriptive rather than quantitative in linking calculated energetics to experimentally observed FE differences. The manuscript would benefit from: A clearer energetic comparison between $2e^-$ and $4e^-$ limiting steps, Correlation between ΔG differences and measured FE values, Consideration of possible mass-transport or bicarbonate-mediated side reactions affecting quantification.

Response: We thank the reviewer for this critical and insightful comment. We fully agree that while reduced charge-transfer resistance, higher K_{trans}/K_{rec} ratios, and increased ECSA can explain improved

activity (higher photocurrent) and stability, they do not inherently account for the enhanced selectivity between the $2e^-$ and $4e^-$ pathways. Selectivity is indeed governed by the relative free energy barriers of competing intermediates and their surface coverage dynamics.

1. **Clearer energetic comparison between $2e^-$ and $4e^-$ limiting steps**

We have supplemented DFT calculations with a direct comparison of the Gibbs free energy profiles for the $2e^-$ WOR (toward H_2O_2) and the $4e^-$ OER (toward O_2) on the photoanode surfaces, as well as for the $2e^-$ ORR versus $4e^-$ ORR on the photocathode surfaces (**Fig. R3a-d**). For the photoanode (Zn-TiO_2/BVO/WO_3 vs. TiO_2/BVO/WO_3 vs. BVO/WO_3), we now report the free energy change of the potential-determining step (PDS) for each pathway:

1) $2e^-$ WOR: the PDS is the formation of $*HCO_4^-$ from $*HCO_3^-$. The ΔG values are -0.17 eV (Zn-TiO_2/BVO/WO_3), +0.31 eV (TiO_2/BVO/WO_3), and +0.46 eV (BVO/WO_3).

2) $4e^-$ OER: the PDS is the formation of *OOH. The ΔG values are +0.49 eV (Zn-TiO_2/BVO/WO_3), +0.47 eV (TiO_2/BVO/WO_3), and +0.39 eV (BVO/WO_3).

The large positive ΔG for the $4e^-$ pathway on Zn-TiO_2/BVO/WO_3 (+0.49 eV) relative to the $2e^-$ pathway (-0.17 eV) creates a $\Delta_{\Delta G}$ of 0.66 eV in favor of the $2e^-$ route, which quantitatively explains the high selectivity.

For the photocathode (Ru:CuO/Nb-CBO vs. CuO/Nb-CBO vs. Nb-CBO), we compare the *OOH stabilization energy ($2e^-$ ORR) versus the *O formation energy ($4e^-$ ORR). The ΔG_{*OOH} for the $2e^-$ pathway is 0.07 eV (Ru:CuO/Nb-CBO), 0.22 eV (CuO/Nb-CBO), and 0.41 eV (Nb-CBO). The ΔG_{*O} for the $4e^-$ pathway is 1.55 eV, 1.46 eV, and 1.44 eV, respectively. The much larger ΔG_{*O} on Ru:CuO/Nb-CBO indicates strong suppression of the $4e^-$ route, while the low ΔG_{*OOH} favors the $2e^-$ pathway.

2. **Size relationship between ΔG differences and measured FE values**

We present a clear size relationship. A lower (more favorable) ΔG for the $2e^-$ pathway corresponds to a higher experimental FE. For the photoanodes, the ΔG values for the key $*HCO_4^-$ intermediate ($2e^-$ WOR) are -0.17 eV for Zn-TiO_2/BVO/WO_3, +0.31 eV for TiO_2/BVO/WO_3, and +0.46 eV for BVO/WO_3; the corresponding FE values are 90%, 74%, and 41% at 1.2 V_{RHE}, respectively. For the photocathodes, the ΔG values for the *OOH intermediate ($2e^-$ ORR) are 0.07 eV for Ru:CuO/Nb-CBO, 0.22 eV for CuO/Nb-CBO, and 0.41 eV for Nb-CBO; the corresponding FE values are 91.9%, 88%, and 58% at 0.6 V_{RHE}, respectively. This relationship confirms that selectivity is governed by the

relative thermodynamic barriers (**Fig. R3e and f**).

3. **Consideration of mass-transport and bicarbonate-mediated side reactions**

We acknowledge that mass transport and the bicarbonate-mediated pathway could affect quantification. To address this, we have performed the following additional experiments and analyses:

1) Mass-transport effects: We repeated the PEC measurements at different stirring rates (0, 300, 600 rpm), and found that the H_2O_2 FE remained unchanged within ±2% for the photoanode and ±1.5% for the photocathode, indicating that mass transport of O_2 or HCO_3^- is not rate-limiting under our conditions (1 M $NaHCO_3$, pH 10, with constant stirring) (**Fig. R3g**).

2) Bicarbonate mediated side reactions: We performed control experiments in HCO_3^- free electrolyte (0.1 M NaOH, pH 10), and observed a drastic drop in H_2O_2 FE from 90.2% to 8.3% for the Zn-TiO_2/BVO/WO_3. This confirms that the bicarbonate/carbonate species are essential mediators, and the reported FE values reflect the true bicarbonate mediated pathway, not an artifact of side reactions (**Fig. R2h**).

4. **Revision of the text to avoid overemphasis on ECSA and impedance.**

We have carefully revised the manuscript to separate the discussion of activity, which benefits from higher ECSA, lower charge-transfer resistance, and faster charge transport, from selectivity which is governed by the relative free energies of intermediates. The text now explicitly states that EIS, IMPS, and ECSA results support the enhanced photocurrent and stability, whereas the selectivity improvement is explained by DFT-derived ΔG values and in situ spectroscopy.

We thank the reviewer for pushing us to provide a more rigorous, quantitative, and mechanism-focused analysis.

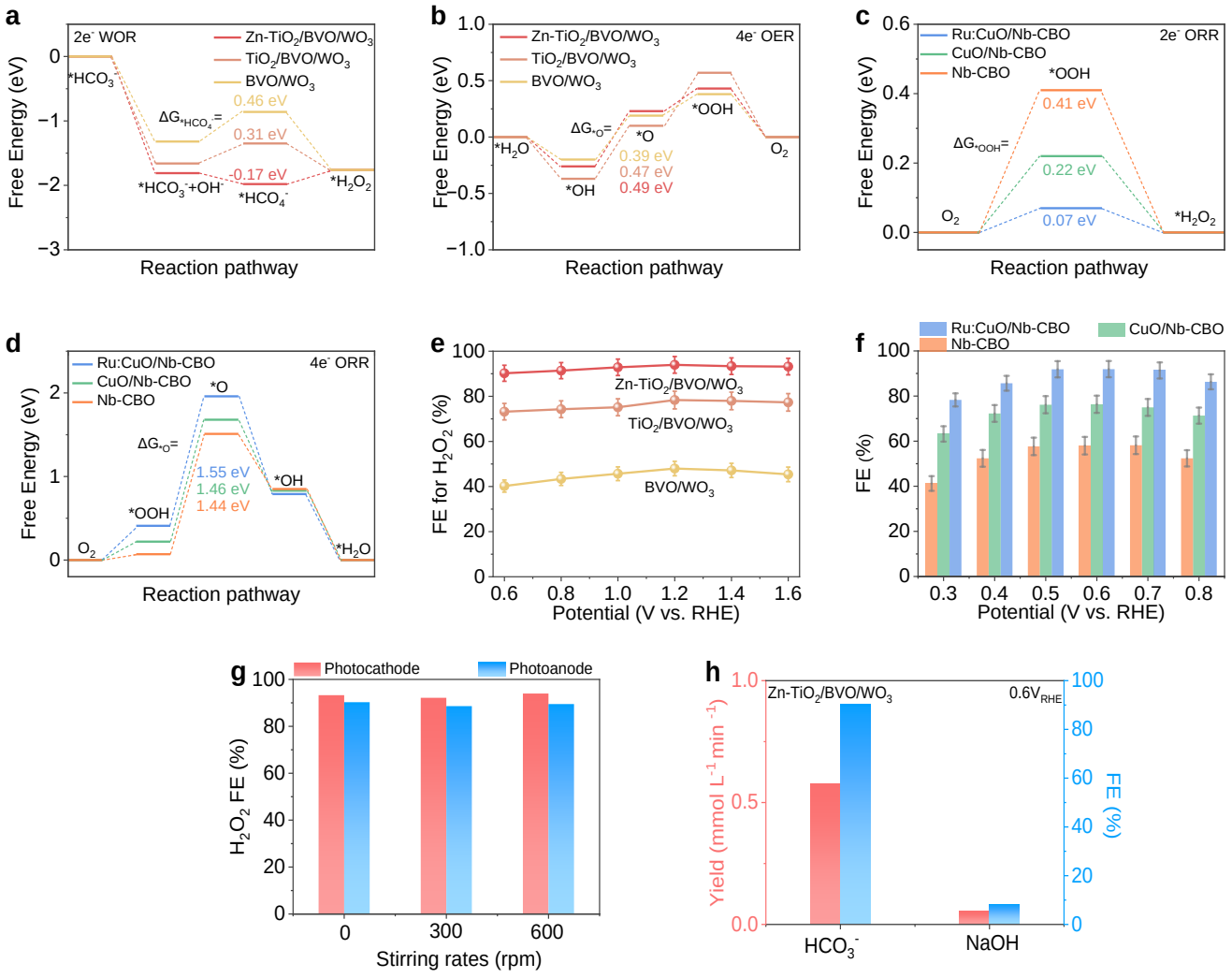

Fig. R3. a 2e⁻ WOR and **b** 4e⁻ OER processes on BVO/WO_3, $TiO_2/BVO/WO_3$, and $Zn\text{-}TiO_2/BVO/WO_3$. **c** 2e⁻ ORR and **d** 4e⁻ OER processes on Nb-CBO, CuO/Nb-CBO, and Ru:CuO/Nb-CBO. **e** FEs of H_2O_2 for BVO/WO_3, $TiO_2/BVO/WO_3$, and $Zn\text{-}TiO_2/BVO/WO_3$ at various applied potentials with a fixed reaction time of 30 min. **f** FEs of H_2O_2 for Nb-CBO, CuO/Nb-CBO, and Ru:CuO/Nb-CBO at various applied potentials with a fixed reaction time of 30 min. **g** FEs of H_2O_2 for photoanode and photocathode at various stirring rates. **h** FEs and yields of H_2O_2 for $Zn\text{-}TiO_2/BVO/WO_3$ at various electrolyte.

Reviewer #4:

We thank the reviewer 4 for the positive comments of our manuscript. We have made the suggested revision.

This manuscript reports a photoelectrochemical bipolar system for hydrogen peroxide (H_2O_2) generation from water (H_2O) and oxygen (O_2), employing a Zn-TiO_2/BVO/WO_3 photoanode and a Ru:CuO/Nb-CBO photocathode. The work demonstrates highly selective and stable H_2O_2 production using H_2O and O_2 as feedstocks.

The findings are highly interesting and novel, and the topic is well aligned with the scope of Nature Communications. However, several points require further clarification before the manuscript can be considered for publication.

1. For Fig. 2 and Fig. 3, I believe that the selectivity (F. E.) data should include the applied charge or the reaction time in the captions.

Response: Thank you for your comment. We have added the applied charge and the corresponding reaction time in the captions of both Fig. 2 and Fig. 3. The selectivity and yield measurements were performed for a fixed reaction time of 60 min.

2. To demonstrate suppression of H_2O_2 decomposition, it is essential to provide long-term time-dependent data for both the anode and cathode reactions, including H_2O_2 production and selectivity (F. E.). In addition, I suggest including a control experiment (decomposition test) in which a high concentration of H_2O_2 is pre-added to evaluate its stability under the reaction conditions.

Response: Thank you for your insightful comment. We fully agree that supplementing long-term time-dependent data and targeted control experiments is critical to verifying the suppression of H_2O_2 decomposition.

1) **Long-term time-dependent data for anode and cathode.** In the revised manuscript, we add new figures showing the time-dependent H_2O_2 production and Faradaic efficiency (FE) over continuous operation. For the photoanode (Zn-TiO_2/BVO/WO_3), we provide a 10-hour continuous test with H_2O_2 concentration and FE measured every hour (**Fig. R1a**). For the photocathode (Ru:CuO/Nb-CBO), we provide a 10-hour continuous test with measurements every hour (**Fig. R1b**).

These results demonstrate that both photoelectrodes maintain stable H_2O_2 production and high FE throughout the entire test duration, with no significant decay.

2) **Control decomposition test with pre-added H_2O_2.** The suggested decomposition control experiment has been performed (**Fig. R1c**). For the photoanode, 0.5 M H_2O_2 was added to the electrolyte (1 M $NaHCO_3$, pH 10) containing the Zn-TiO_2/BVO/WO_3 electrode under illumination at 0.6 V_{RHE}. For the photocathode, a similar test was conducted under ORR conditions (O_2-saturated electrolyte, 0.6 V_{RHE}, illumination). After 2 hours, the H_2O_2 concentrations in the presence of the photoanode or photocathode showed no significant difference from those in the absence of any photoelectrode (blank control). This confirms that neither the photoanode nor the photocathode causes additional H_2O_2 decomposition.

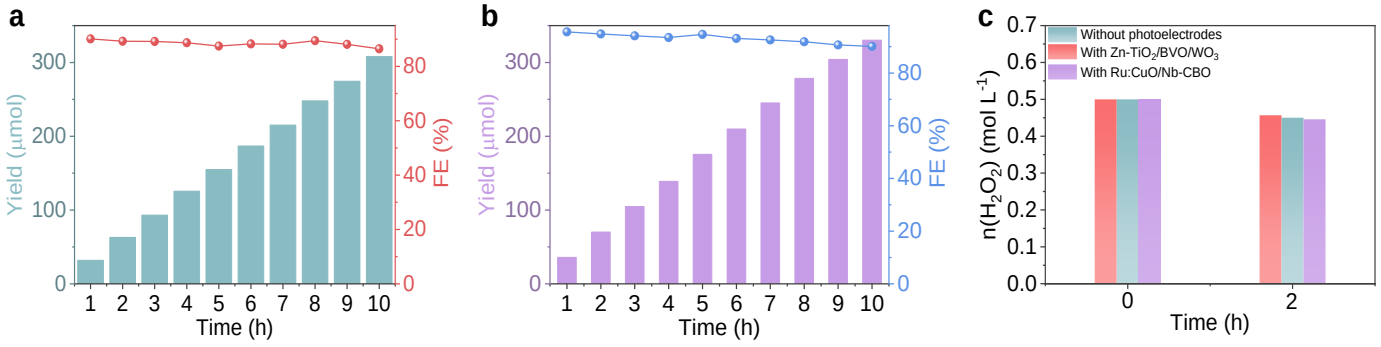

Fig. R1. a Accumulated H_2O_2 yields and FEs on Zn-TiO_2/BVO/WO_3 during 10 h operation. **b** Accumulated H_2O_2 yields and FEs on Ru:CuO/Nb-CBO during 10 h operation. **c** Control decomposition tests with pre-added H_2O_2.

3. In Fig. 2(a), the onset potentials for Zn-TiO_2/BVO/WO_3 and TiO_2/BVO/WO_3 are observed at more negative biases than+0.4 V vs. RHE (onset potential of +0.31 V vs. RHE in Zn-TiO_2/BVO/WO_3). Could the authors kindly clarify the reason for this behavior? If photoexcited electrons generated in $BiVO_4$ are transferred to FTO through the conduction band of WO_3, the onset potential would be expected to correspond to the conduction band minimum of WO_3. How do the authors interpret the observed onset potentials in this context?

Response: We thank the reviewer for this insightful question regarding the onset potentials of the photoanodes. To clarify this point, we have re-measured the conduction band minima (CBM) of the individual materials using ultraviolet photoelectron spectroscopy (UPS) (**Fig. R2a-c**). The results show that the CBM of WO_3 is 0.46 V_{RHE}, that of $BiVO_4$ is 0.04 V_{RHE}, and that of TiO_2 is -0.95 V_{RHE}.

Based on these values, a simple type-II heterojunction between $BiVO_4$ and WO_3 would indeed suggest an onset potential near 0.46 V_{RHE}. However, the observed onset potential for Zn-TiO_2/BVO/WO_3 is 0.31 V_{RHE}, which is significantly more negative. This cathodic shift can be explained by several factors.

1) The onset potential in a photoelectrochemical system is not simply equal to the conduction band minimum of the back contact layer.[1] Under illumination, the quasi-Fermi level of electrons shifts toward the conduction band, and the photocurrent onset is determined by the competition between charge transfer to the electrolyte and surface recombination. The type-II heterojunction between $BiVO_4$ and WO_3 creates a built-in electric field that drives electrons from $BiVO_4$ to WO_3 and holes in the opposite direction. This field enhances charge separation and reduces surface recombination, effectively lowering the overpotential required to collect photogenerated holes at the surface.[2]

2) The TiO_2 passivation layer and Zn doping further modify the surface band bending. The TiO_2 layer has a very low CBM (-0.95 V_{RHE}), which acts as a strong electron acceptor. This is evidenced by the positive shifts in Bi 4f and V 2p XPS core levels, indicating electron extraction from $BiVO_4$ (**Fig. R2d and e**). This extraction increases the band bending at the $BiVO_4$/electrolyte interface, facilitating hole migration to the surface and suppressing electron back-recombination. The Zn doping introduces shallow donor states that increase carrier density and improve conductivity, as supported by the higher charge transport rate constants from IMPS (**Fig. R2f**).

References

[1] Dong, C., Yang, Y., Hu, X., Cho, Y., Jang, G., Ao, Y., Wang, L., Shen, J., Park, J. H., Zhang, K. Self-cycled photo-Fenton-like system based on an artificial leaf with a solar-to-H_2O_2 conversion efficiency of 1.46%. *Nat. Commun.* **13**, 4982 (2022).

[2] Chen, S., Chen, Y., Zhang, H., Abbas, M., Ren, D., Chen, Y., Luo, J., Zheng, Z., Su, Z., Liang, G. (Zn,Ti)O Electron Transport Layer Enables the Highest Conversion Efficiency in Cd-Free Sb_2Se_3 Photocathodes for Stable Solar Hydrogen Production. *Adv. Mater*. **38**, e18202 (2026).

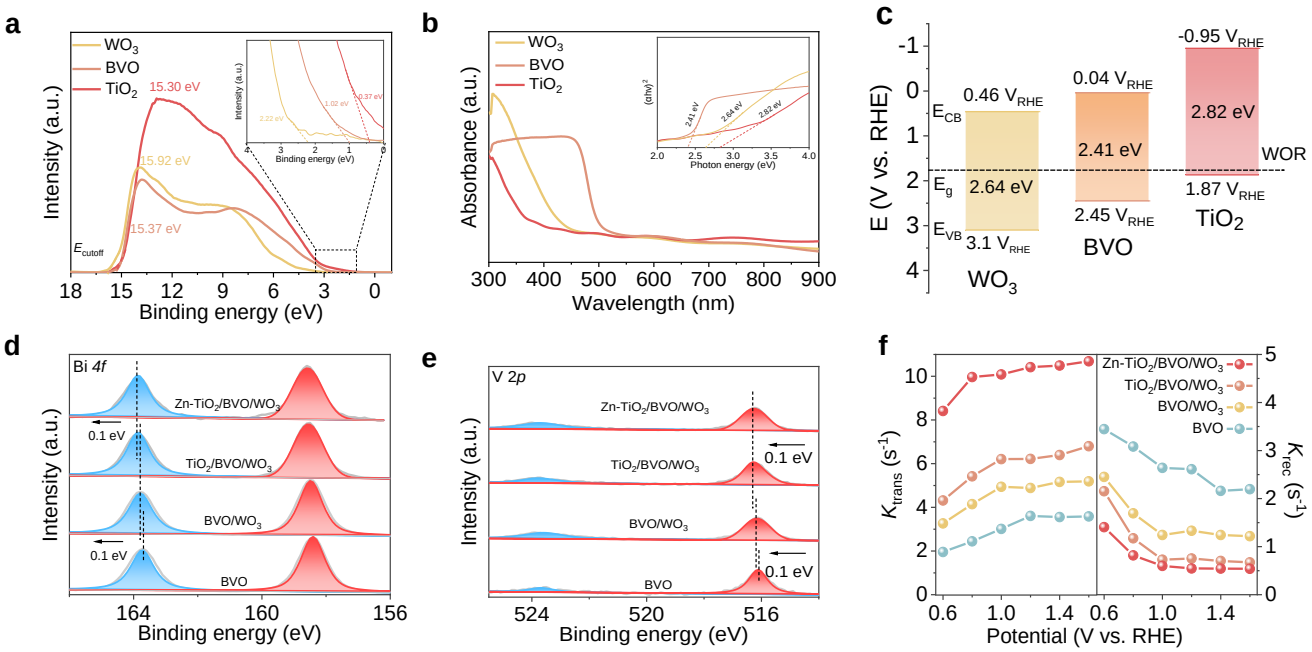

Fig. R2. a UPS measurements of TiO_2, BVO and WO_3. Inset shows the zoomed-in image area in the black dashed lines. **b** UV-vis spectra of TiO_2, BVO and WO_3. Inset shows the optical band gaps. **c** Band alignments of TiO_2, BVO and WO_3. **d** Bi *4f* XPS and **e** V *2p* XPS spectra of photoanodes. **f** Charge transfer (k_{trans}) and charge recombination (k_{rec}) rate constants from IMPS spectra.

4. In the mechanistic analysis in the main text, the high performance (high selectivity) of Zn-TiO_2/BVO/WO_3 is attributed to the strongest adsorption affinity of HCO_4^-. However, the reason why the two-electron oxidation of H_2O_2 (+0.68 V vs. RHE), which is thermodynamically easier than the two-electron oxidation of H_2O (+1.77 V vs. RHE), is largely suppressed is not entirely clear to me. I would appreciate a more detailed explanation of the direct mechanism responsible for this suppression.

Response: We appreciate the reviewer's valuable question. We now provide a detailed mechanistic explanation for the effective suppression of H_2O_2 two-electron oxidation on the Zn-TiO_2/BVO/WO_3 photoanode, which is primarily attributed to the preferential and strong adsorption of bicarbonate/carbonate species on the photoanode surface (rather than H_2O_2 molecules) and the Zn doping-induced electronic structure modulation of the TiO_2 layer.

1) For the in-situ IR spectroscopy tests, we conducted parallel experiments in 0.1 mM NaOH (pH=10) and 1 M $NaHCO_3$ + NaOH (pH=10) under the same $2e^-$ WOR reaction conditions (**Fig. R3a and b**). In the electrolyte with bicarbonate, distinct characteristic peaks of surface-adsorbed HCO_3^- (≈1650 cm^{-1}) and CO_3^{2-} (≈1400 cm^{-1}) are clearly observed on the Zn-TiO_2/BVO/WO_3 surface, and the

peak intensities increase significantly with the applied bias. These peaks maintain high intensity throughout the reaction process, confirming the sustained and preferential adsorption of bicarbonate/carbonate species on the photoanode active sites. In contrast, in the bicarbonate-free 0.1 mM NaOH electrolyte, no obvious adsorption peaks of inorganic anions are detected on the photoanode surface, while only a weak peak assigned to the *OOH intermediate (≈1200 cm^{-1}) appears with increasing bias, accompanied by a significant decrease in H_2O_2 FE (from 90.2% in $NaHCO_3$ + NaOH to 8.3% in NaOH). This direct spectral comparison demonstrates that bicarbonate/carbonate species occupy the dominant active sites of the photoanode, effectively inhibiting the adsorption of H_2O_2 molecules on the surface and thus blocking the subsequent two-electron oxidation of H_2O_2.

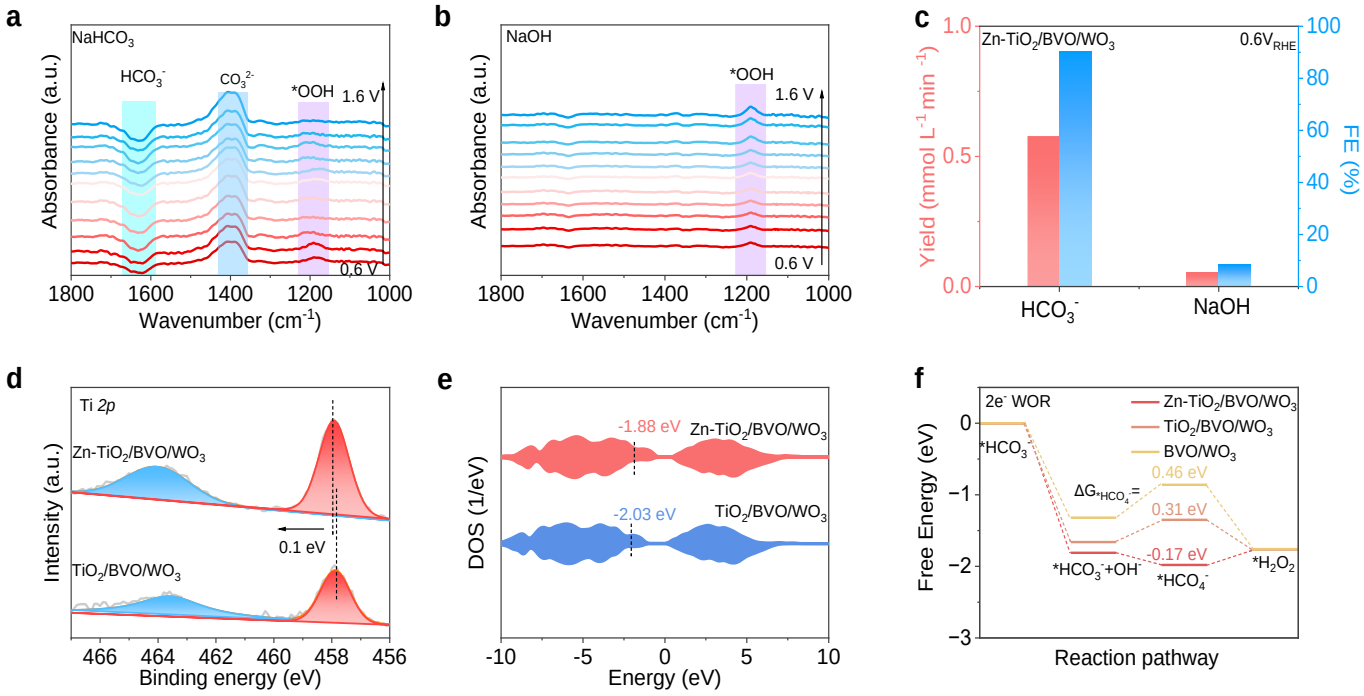

Fig. R3. a,**b** In situ ATR-SEIRAS spectra of adsorbed intermediates recorded on Zn-TiO_2/BVO/WO_3 in **a** 1 M $NaHCO_3$ and **b** 0.1 mM NaOH. **c** FEs and yields of H_2O_2 at various electrolytes. **d** Ti *2p* XPS spectra of TiO_2/BVO/WO_3 and Zn-TiO_2/BVO/WO_3. **e** Total DOS of surface states for TiO_2/BVO/WO_3 and Zn-TiO_2/BVO/WO_3.**f** 2e^- WOR processes on BVO/WO_3, TiO_2/BVO/WO_3, and Zn-TiO_2/BVO/WO_3.

2) In addition, Zn doping in the TiO_2 layer further reinforces the suppression of H_2O_2 oxidation by modulating the surface electronic structure of the photoanode. As confirmed by XPS and DFT calculations, Zn doping induces a positive shift of the Ti 2p core level and an upshift of the Ti d-band center, which enhances the adsorption affinity of the photoanode for HCO_3^- ($\Delta G^*HCO_4^-$ = -0.15 eV)

while reducing the interaction between the photoanode surface and H_2O_2 molecules (**Fig. R3d-f**). This electronic structure regulation makes the preferential adsorption of bicarbonate species more thermodynamically favorable, and the formed stable $*HCO_4^-$ intermediate (the key mediator for $2e^-$ WOR to H_2O_2) further sterically hinders H_2O_2 from approaching the active sites and undergoing oxidation.

This mechanistic behavior is also consistent with relevant literature reports on bicarbonate-mediated photoelectrochemical H_2O_2 synthesis systems, where the preferential adsorption of bicarbonate/carbonate anions on the semiconductor photoanode surface is proven to be a universal and effective strategy to suppress H_2O_2 anodic oxidation and improve H_2O_2 selectivity.

5. It may strengthen the discussion to include citations on H_2O_2 generation via HCO_3^- oxidation, such as the following references.

K. Sayama et. al., Chem. Commun., 2016, 52, 5406-5409

K. Sayama et. al., Chem. Asian J., 2017, 12, 1111-1119

H. Kusama et. al., Phys. Chem. Chem. Phys., 2022, 24, 5894-5902

Response: Thank you for your valuable comment and recommended references. We have added the cited studies on H_2O_2 generation via HCO_3^- oxidation to the corresponding discussion section of the revised manuscript, which strengthens the mechanistic elaboration of our work. All references are formatted in line with the journal's requirements.

Reviewer #5:

We thank the reviewer 5 for the positive comments of our manuscript. We have made the suggested revision.

In this manuscript, the authors report a well-designed bias-free PEC tandem system with impressive total FE (>170%) for H_2O_2 production. The integration of Zn–TiO_2/$BiVO_4$/WO_3 and Ru:CuO/Nb-CBO is scientifically sound, and the extensive in situ spectroscopic analysis convincingly supports the proposed mechanistic pathways. The authors provide strong evidence that heterojunction engineering and intermediate regulation suppress $4e^-$ pathways while stabilizing key *OOH species. However, several points require clarification: (1) The reported combined FE >170% should be explicitly discussed in terms of system-level accounting (dual-electrode contribution vs. theoretical limits). (2) Long-term stability beyond 10–50 h is still limited for practical deployment; degradation pathways should be analyzed. (3) The bicarbonate-mediated 2e WOR mechanism needs clearer differentiation between true catalytic pathways and solution-phase reactions. (4) Outdoor sunlight data would benefit from reporting irradiance variability. Thus, I would like to recommend the manuscript to be accepted after revision, and the authors should also address the following comments.

Response: We thank the reviewer for the insightful questions.

1) Regarding the system-level accounting of the combined FE >170%: We have explicitly defined the total Faradaic efficiency (FE) as Total FE = $2F\ (n_{anode} + n_{cathode})/Q_{total} \times 100\%$. Because the same photogenerated electrons drive both the $2e^-$ WOR at the anode and the $2e^-$ ORR at the cathode, the theoretical maximum total FE is 200% when both half-reactions are 100% selective. Our measured value of 171.7% does not violate charge conservation, nor does it imply a single-electrode FE exceeding 100%. We have provided a strict electron-balance verification and added a clear discussion in the revised manuscript.

2) On the long-term stability and degradation pathways: We have performed ICP-MS, XPS, and SEM analyses on the aged electrodes. The results show selective leaching of Zn and Ti from the photoanode (after 10 h) and Ru and Cu from the photocathode (after 50 h), while the core heterojunctions (BVO/WO_3 and Nb-CBO) remain intact. This partial dissolution of the surface modifier layers (Zn-TiO_2 and Ru:CuO) is the primary cause of the gradual FE decline (from 90.2% to ~88.1% for the anode, and from 91.9% to ~86.4% for the cathode). In contrast, the photocurrent

remains relatively stable because the intact heterojunctions maintain efficient charge transport.

3) For distinguishing the bicarbonate-mediated 2e$^-$ WOR mechanism from direct water oxidation: we performed parallel in situ ATR-SEIRAS tests in bicarbonate-containing (1 M $NaHCO_3$, pH=10) and bicarbonate-free (0.1 mM NaOH, pH=10) electrolytes. In the presence of bicarbonate, clear surface-adsorbed HCO_3^- (~1650 cm^{-1}) and CO_3^{2-} (~1400 cm^{-1}) peaks were observed, while in its absence only a weak *OOH peak (~1200 cm^{-1}) appeared and the H_2O_2 FE dropped from 90.2% to 8.3%. This confirms that the reaction proceeds via the bicarbonate-mediated pathway rather than direct water oxidation.

4) Regarding outdoor sunlight data and irradiance variability: We have now provided the average irradiance (72 mW cm^{-2}, 0.72 sun) measured during the outdoor tests. Additionally, we performed three independent repeated measurements under varying natural sunlight intensities, and the photocurrent showed a strong linear correlation (R^2 = 0.996) with the real-time irradiance, confirming good reproducibility and system robustness under fluctuating sunlight conditions.

1. The authors are suggested to provide more information about the validation of the Ce^{4+} colorimetric H_2O_2 quantification against matrix effects (high carbonate/bicarbonate, high pH) and possible oxidants/reductants.

Response: We thank the reviewer for this valuable suggestion. To validate the reliability of the Ce^{4+} colorimetric method under our experimental conditions (1 M $NaHCO_3$, pH=1), we performed the following control experiments.

1) We established calibration curves for H_2O_2 quantification using both the Ce^{4+} colorimetric method and the DPD (N,N-diethyl-p-phenylenediamine) method.[1-4] Both methods showed excellent linearity (R^2=0.997) over the concentration range relevant to our measurements (**Fig. R1a-d**).

2) We selected Zn–TiO_2/$BiVO_4$/WO_3 photoanode after 1 h of operation at 0.6 V_{RHE}, and quantified H_2O_2 simultaneously using the Ce^{4+} method and the DPD method (**Fig. R1e**). The results obtained from the two methods agreed within a relative error of ±5%. This good agreement confirms that the Ce^{4+} colorimetric method is accurate under our specific reaction conditions.

3) We assessed potential interference from oxidants or reactive species present in the system. The only possible oxidants in the electrolyte are dissolved O_2 and H_2O_2 itself. After mixing the electrolyte with the acidic Ce^{4+} solution, O_2 does not react with Ce^{4+} under the measurement conditions.

To test for possible interference from carbonate-derived peroxymonocarbonate or other reactive oxygen species, we performed a control experiment: adding 1 mM Na_2CO_3 or 1 mM $NaHCO_3$ to a standard H_2O_2 solution (20 μM) did not change the absorbance at 317 nm (the characteristic absorption peak of Ce^{4+}) within experimental error (**Fig. R1f**). This confirms that neither carbonate/bicarbonate ions nor their derivatives interfere with the Ce^{4+}-based assay.

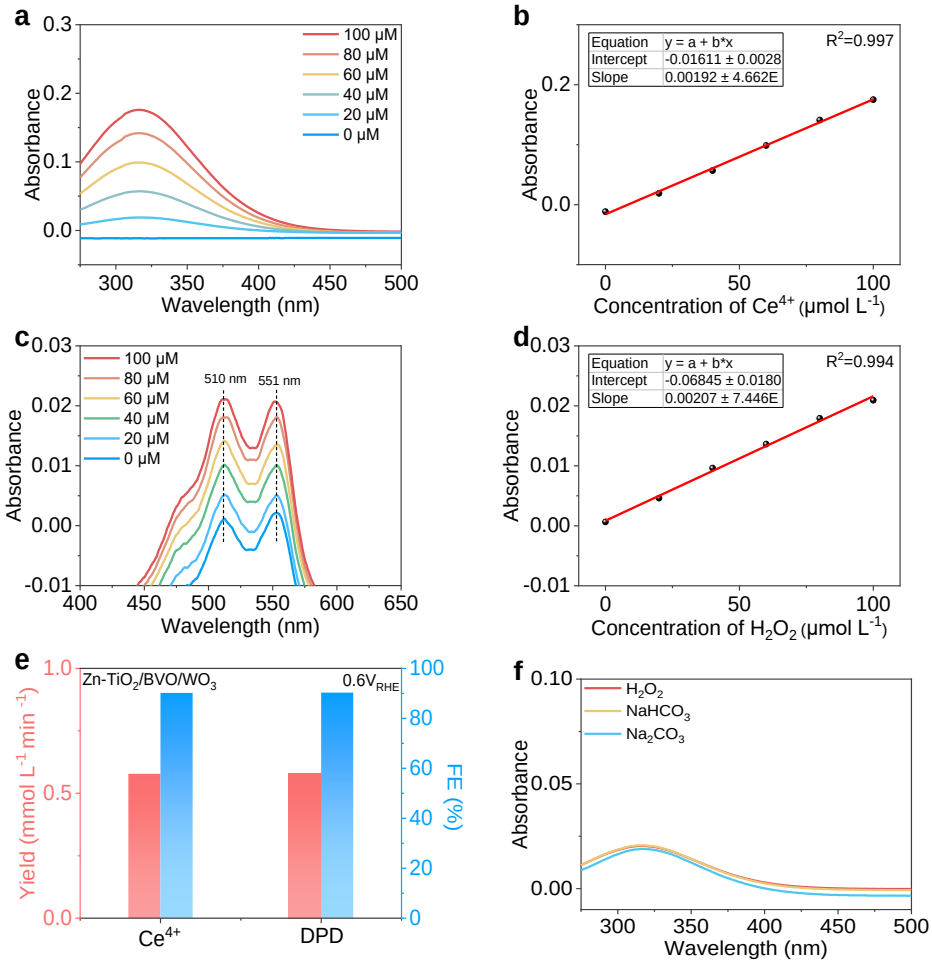

Fig. R1. a UV-visible absorption spectra for various Ce^{4+} concentrations. **b** Fitting results of the absorbance vs. concentration. **c** The base of verification using standard 0 to 100 μM H_2O_2. **d** Fitting results of the absorbance vs. concentration. **e** Quantified H_2O_2 simultaneously using the Ce^{4+} method and the DPD method. **f** Absorbance curves of 20 μM H_2O_2 in various electrolytes.

References

[1] Sun, Y., Fan, K., Wang, L., Yang, Y., Li, Z., Shao, M., Duan X. Boosting electrochemical oxygen reduction to hydrogen peroxide coupled with organic oxidation. *Nat. Commun.* **15**, 6098 (2024).

[2] Yan, M., Yang, H., Gong, Z., Zhu, J., Allen, C., Cheng, T., Fei, H. Sulfur-Tuned Main-Group Sb–N–C Catalysts

for Selective 2-Electron and 4-Electron Oxygen Reduction. *Adv. Mater.* **36**, 2402963 (2024).

[3] Moon, S., Park, Y. S., Lee, H., Jeong, W., Kwon, E., Lee, J., Yun, J., Lee, S., Kim, J. H., Yu, S., Moon, J. Unassisted photoelectrochemical hydrogen peroxide production over MoOx-supported Mo on a Cu_3BiS_3 photocathode. *Energy Environ. Sci.* **17**, 5588 (2024).

[4] Mehrotra, R., Oh, D., Jang, J.-W. Unassisted selective solar hydrogen peroxide production by an oxidised buckypaper-integrated perovskite photocathode. *Nat. Commun.* **12**:6644 (2021).

2. Regarding the mass balance and the crossover in the tandem cell, the authors should provide the detailed measurement of H_2O_2 crossover rate and any parasitic decomposition on the opposite electrode (with/without PEM). It would be good if the compartment concentrations vs time, membrane type/thickness can also be reported.

Response: We thank the reviewer for this constructive suggestion. We have performed additional experiments to systematically evaluate H_2O_2 crossover and mass balance in unbiased tandem cell. The key findings are summarized below.

1) **Membrane type and thickness.** A proton exchange membrane (PEM, Nafion 117, 183 μm thick, Ion Power Inc.) was used in the two-compartment cell to separate the anolyte and catholyte. Before use, the membrane was pretreated by boiling sequentially in 3% H_2O_2, deionized water, 0.5 M H_2SO_4, and again in deionized water (each for 1 h).[1] The effective membrane area was 1 cm^2.

2) **Measurement of H_2O_2 crossover rate (with PEM).** We assembled the tandem cell with the PEM and filled the anode and cathode compartments each with 30 mL of 1 M $NaHCO_3$ (pH=10). A known amount of H_2O_2 (50 μM initial concentration) was spiked into the anode compartment while the cathode compartment contained no H_2O_2 initially. The cell was kept under AM 1.5G illumination without applied bias (open circuit). Samples were taken from the cathode compartments at regular intervals (0, 10, 20, 30, 40, 50, and 60 min) and analyzed by the Ce^{4+} colorimetric method.

The H_2O_2 concentration in the cathode compartment increased linearly over time (**Fig. R2**). The crossover flux was calculated as:

$$J_{crossover} = \frac{V_{cathode} \times dC_{cathode}/d_t}{A_{membrane}}$$

where $V_{cathode}$=30 mL, $A_{membrane}$=1 cm^2, and $dC_{cathode}/dt$ is the slope (0.03 μM min^{-1}). The obtained crossover rate is 9×10^{-10} mol cm^{-2} min^{-1}. This value is extremely low (equivalent to a

cross-over of <0.3% of the total H_2O_2 produced over 1 h), confirming that the PEM effectively suppresses H_2O_2 crossover under our operating conditions.

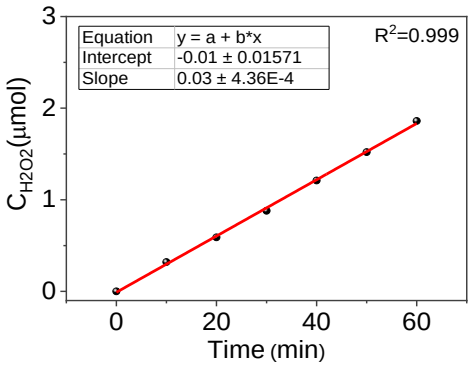

Fig. R2. Plot of H_2O_2 concentration in the cathode compartment as a function of time with PEM.

Reference

[1] Oh, D., Hwang, S. W., Kim, D. Y., Matthews, J. E., Lee, J., Acosta, J. E. A., Lee, S.-W., Xu, Y., Cho, A., Lee, D. U., Jaramillo, T. F., Seo, D.-H., Jang, J.-W. Unassisted electrochemical H_2O_2 production coupled to glycerol oxidation. *Nat. Synth.* **4**, 931-939 (2025)

3. It is beneficial to show the system-level FE calculation (anode + cathode yields, charge passed at each electrode, normalization basis) and provide an error/uncertainty estimate. This would help to dismiss confusion about "exceeding 100%".

Response: We thank the reviewer for the essential suggestion. We agree that a transparent definition of the system-level H_2O_2 yield and a rigorous uncertainty analysis are necessary to avoid any misunderstanding of the "exceeding 100%" statement.

1) **Two-compartment H-cell with proton exchange membrane (PEM).** In our laboratory H-cell (Nafion 117, **Fig. 4b-e**), the anode and cathode are physically separated. The charge passing through the external circuit is identical for both electrodes ($Q_{total} = Q_{anode} = Q_{cathode}$). Each electrode's FE is calculated independently against its own half-reaction, and the theoretical maximum per electrode is 100%.[1,2] Our measured FEs are ~90% (photoanode) and ~92% (photocathode), both below 100%.

2) **Unassisted outdoor single-compartment cell (no membrane).** Under natural sunlight, we used a PEM-free cell (**Fig. 4f and 4g**). Both electrodes share the same electrolyte. The same photogenerated electrons drive both half-reactions: at the anode ($2e^-$ WOR) and at the cathode ($2e^-$ ORR). Consequently, each electron passing through the circuit enables the production of one H_2O_2

molecule at each electrode, giving a theoretical maximum combined yield of **200%** when both half-reactions are 100% selective.[3,4] For this configuration, we define the system-level "total FE" as:

$$\text{Total FE} = \frac{2F(n_{anode}+n_{cathode})}{Q_{total}} \times 100\%$$

where n_{anode} and $n_{cathode}$ are the amounts of H_2O_2 produced at the photoanode and photocathode, respectively, and Q_{total} is the total charge recorded by the external circuit. This definition avoids double-counting charge and strictly adheres to charge conservation, because Q_{total} represents the only charge loop driving both half-reactions simultaneously. The individual FE of each electrode, when calculated against its own half-reaction charge, remains ≤100% (e.g., ~90% for the anode and ~92% for the cathode). The combined value of ~170% simply reflects that the same charge produces H_2O_2 at both electrodes.

3) We provide strict electron-balance verification to validate the rationality of the total FE value. We calculated the total theoretical electron consumption $2F(n_{anode}+n_{cathode})$ from measured H_2O_2 yields and compared it with the experimentally recorded Q_{total}. The relative error between the calculated electron amount and the measured circuit charge is < 3%, confirming strict charge conservation in the system. The total FE of ~170% arises because both electrodes convert the same loop charge into the target $2e^-$ product, rather than any violation of electrochemical fundamentals.

References

[1] Jeon, T. H., Kim, H., Kim, H., Choi, W. Highly durable photoelectrochemical H_2O_2 production via dual photoanode and cathode processes under solar simulating and external bias-free conditions. *Energy Environ. Sci.* **13**, 1730 (2020).

[2] Jeon, T. H., Koo, M. S., Kim, H., Choi, W. Dual-Functional Photocatalytic and Photoelectrocatalytic Systems for Energy- and Resource-Recovering Water Treatment**.** *ACS Catal.* **8**, 11542-11563 (2018).

[3] Wang, Z., Li, K., Hu, J., Li, A., Tang, Y., Sun, Y., Wan, P., Jiang, H., Chen, Y. Dual-Functional Catalyst of Amorphous TiO_2 Embedded in Mesoporous Carbon Hollow Spheres for H_2O_2 Electrosynthesis. *Adv. Funct. Mater.* **35**, 2425301 (2025).

[4] Yan, M., Yang, H., Gong, Z., Zhu, J., Allen, C., Cheng, T., Fei, H. Sulfur-Tuned Main-Group Sb−N−C Catalysts for Selective 2-Electron and 4-Electron Oxygen Reduction. *Adv. Mater.* **36**, 2402963 (2024).

4. It is recommended that the authors should have more insightful discussion on how they distinguish

direct 2e⁻ WOR from bicarbonate-mediated solution pathways.

Response: Thank you for your professional suggestion. We have conducted targeted investigations to distinguish direct 2e⁻ WOR from bicarbonate-mediated solution pathways. We performed parallel in situ infrared spectroscopy tests in 1 M $NaHCO_3$ (pH=10) and in 0.1 mM NaOH (pH=10, bicarbonate-free) under the same 2e⁻ WOR reaction conditions (**Fig. R3a and b**). In the bicarbonate-containing electrolyte, distinct characteristic peaks of surface-adsorbed HCO_3^- (≈1650 cm^{-1}) and CO_3^{2-} (≈1400 cm^{-1}) are clearly observed on the Zn-TiO_2/BVO/WO_3 surface, and the peak intensities increase significantly with applied bias. These peaks maintain high intensity throughout the reaction, confirming the sustained and preferential adsorption of bicarbonate/carbonate species on the photoanode active sites. In contrast, in the bicarbonate-free 0.1 mM NaOH electrolyte, no obvious adsorption peaks of inorganic anions are detected on the photoanode surface, while only a weak peak assigned to the *OOH intermediate (≈1200 cm^{-1}) appears with increasing bias, accompanied by a significant decrease in H_2O_2 FE (from 90.2% in $NaHCO_3$ to 8.3% in NaOH). This spectroscopic evidence confirms that the reaction proceeds via the bicarbonate-mediated mechanism rather than direct water oxidation. We thank you for the reviewer's comments again.

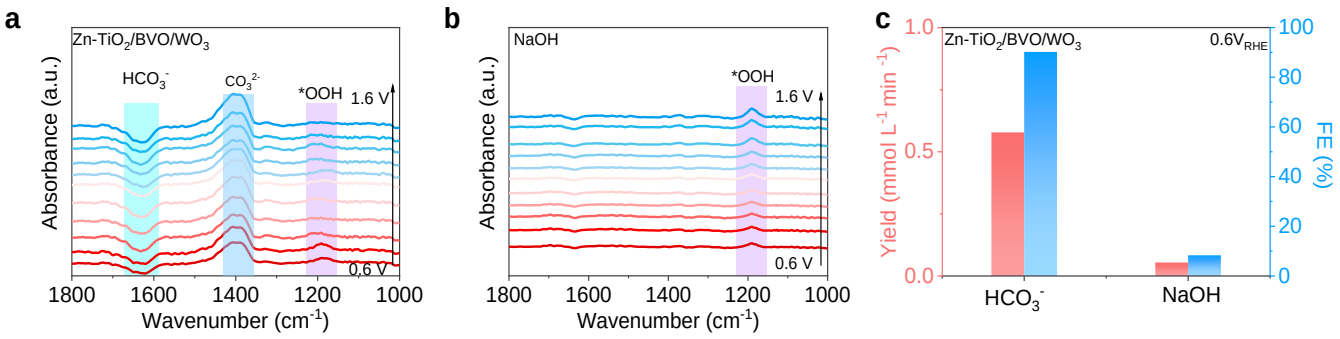

Fig. R3. a, b *In situ* ATR-SEIRAS spectra of adsorbed intermediates recorded on Zn-TiO_2/BVO/WO_3 in **a** 1 M $NaHCO_3$ (pH=1) and **b** 0.1 mM NaOH (pH=10). **c** FEs and yields of H_2O_2 at various electrolytes.

5. By evaluating the catalyst after 10–50 hours of electrolysis via ICP-MS, XPS, and electron microscopy, what evidence of degradation (e.g., leaching or cocatalyst detachment) becomes apparent? How do these physical changes explain the subsequent performance drift in terms of current and Faradaic Efficiency?

Response: We thank the reviewer for this question. Post-stability characterization of the electrodes after stability reveals degradation primarily in the surface functional layers (Zn-TiO_2 on the

photoanode and Ru:CuO on the photocathode), while the underlying heterojunctions remain intact.

1) **ICP-MS analysis** of the electrolytes after long-term tests shows measurable concentrations of Zn and Ti leached from the Zn-TiO_2/BVO/WO_3 photoanode after 10 h, and Ru and Cu leached from the Ru:CuO/Nb-CBO photocathode after 50 h (**Table R1**). All other elements (V, Bi, W, and Nb) remain below 0.05 mg/L, confirming the selective dissolution of the Zn-TiO_2 and Ru:CuO components.

2) **XPS measurements** on the photoanode after 10 h testing reveal that the peak intensities of Zn and Ti decrease significantly compared to the fresh electrode (**Fig. R4a-d**). For the photocathode after 50 h testing, the peak intensities of Ru and Cu also show a clear decline. These reductions in XPS signal intensity are consistent with the partial leaching of the corresponding elements observed by ICP-MS analysis.

3) **SEM imaging** shows no obvious morphological changes for either electrode after stability testing, confirming that the BVO/WO_3 and Nb-CBO heterojunction frameworks remain structurally stable (**Fig. R4e and f**).

4) **Correlation with performance change.** The partial leaching of Zn and Ti from the photoanode reduces the selectivity of the $2e^-$ WOR, causing a sightly decline in H_2O_2 FE from 90.2% to ~88.1% after 10 h (**Fig. R4g**). The loss of Ru and Cu from the photocathode similarly lowers the $2e^-$ ORR selectivity, FE from 91.9% to ~86.4% after 50 h (**Fig. R4h**). In contrast, the photocurrent remains relatively stable because the intact BVO/WO_3 and Nb-CBO heterojunctions maintain efficient charge separation and transport. Thus, the observed performance change is mainly attributed to degradation of the surface modifier layers rather than the core heterojunction structures.

Table R1 ICP analysis of electrolytes for Zn-TiO_2/BVO/WO_3 after 10 h i-t measurements and Ru:CuO/Nb-CBO after 50 h i-t measurements.

Sample	Zn (mg/L)	Ti (mg/L)	V (mg/L)	W (mg/L)	Bi (mg/L)	Cu (mg/L)	Ru (mg/L)	Nb (mg/L)
Zn-TiO_2/BVO/WO_3	0.17	0.38	0.03	0.01	0.03	---	---	---
Ru:CuO/Nb-CBO	---	---	---	---	0.02	0.34	0.18	0.03

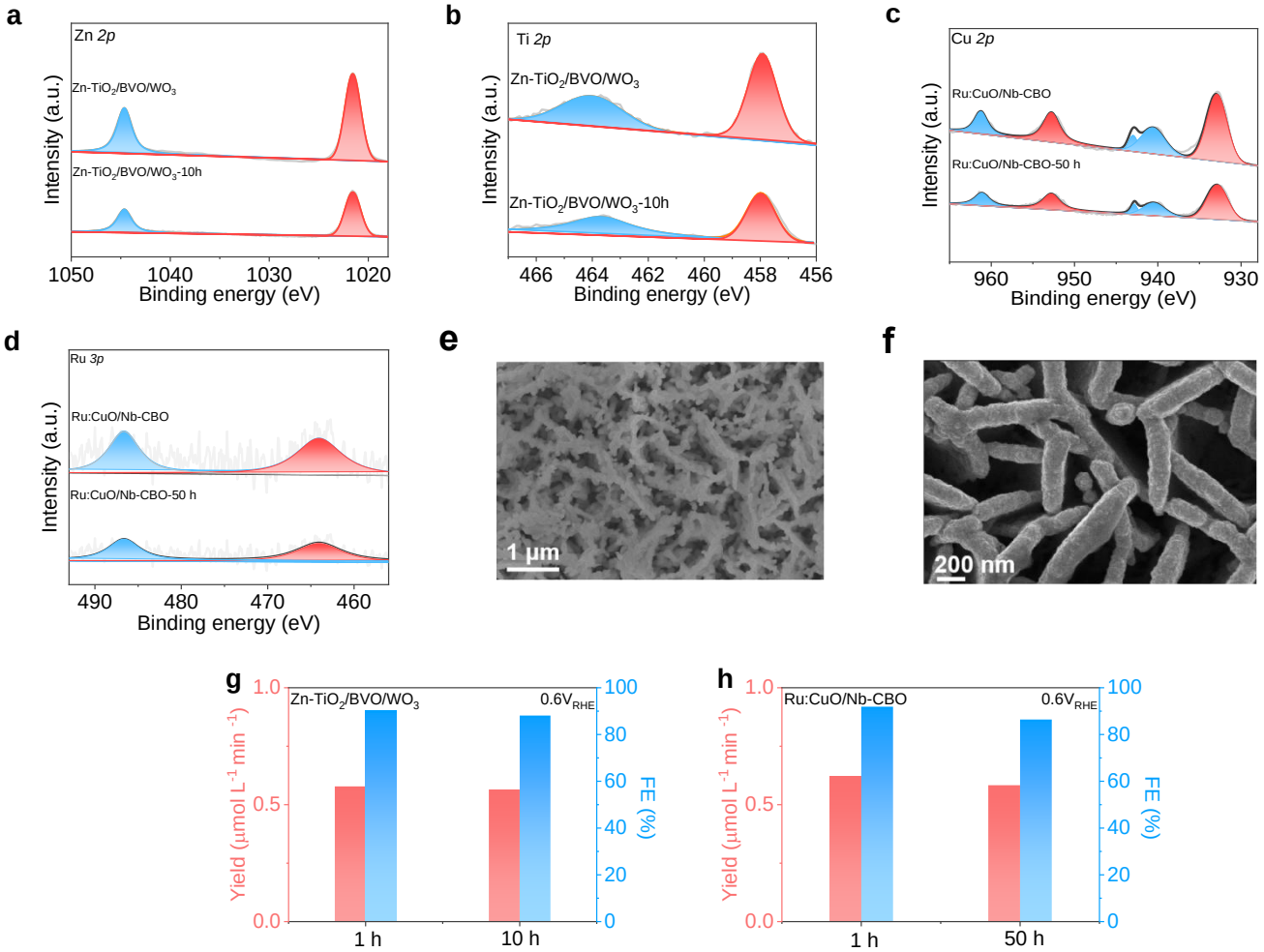

Fig. R4. a Zn *2p* and **b** Ti *2p* XPS spectra of Zn-TiO_2/BVO/WO_3 before and after stability tests. **c** Cu *2p* and **d** Ru *3p* XPS spectra of Ru:CuO/Nb-CBO before and after stability tests. **e** SEM image for Zn-TiO_2/BVO/WO_3 after 10 h stability. **f** SEM image for Ru:CuO/Nb-CBO after 50 h stability. **g** FEs and yields of H_2O_2 of Zn-TiO_2/BVO/WO_3 before and after 10 h stability tests. **h** FEs and yields of H_2O_2 of Ru:CuO/Nb-CBO before and after 50 h stability tests.

6. While outdoor field tests demonstrate stable FE, the resulting bulk concentrations remain in the micromolar range. To better contextualize these findings, please incorporate areal production rates and solar-to-chemical efficiency metrics. Furthermore, evaluate these results against application-specific benchmarks—such as the mg/L thresholds required for effective disinfection.

Response: We thank the reviewer for the suggestion. We sincerely apologize for the mistake on the description of 4.5 μmol L^{-1}. This was a description error in the original manuscript, and the correct concentration should be 7.64 mmol L^{-1} (mM). We have corrected this in the revised manuscript. We have now calculated the areal H_2O_2 production rate and the solar-to-chemical conversion efficiency

(SCC) for both the laboratory (AM 1.5G, 2 cm^2 electrodes) and outdoor (natural sunlight, 20 cm^2 and 36 cm^2 electrodes) tests. We also compare the obtained H_2O_2 concentration with typical disinfection requirements.

1) Areal production rate and solar-to-chemical efficiency. Outdoor tests were performed under natural sunlight with an average intensity of 72 mW cm^{-2} (0.72 sun). The electrolyte volume was 100 mL in a single-compartment (PEM-free) cell. Two sets of photoelectrodes (Zn-TiO_2/BVO/WO_3 anode + Ru:CuO/Nb-CBO cathode) with different areas were tested for 1 h. The results are summarized in the table below.[1,2]

The areal H_2O_2 production rate (R_A, in μmol cm^{-2} h^{-1}) is defined as:

$$R_A = \frac{C \times V}{A \times t}$$

where C is the measured H_2O_2 concentration (μmol L^{-1}), V is the electrolyte volume (L), A is the total geometric area of the photoelectrode (cm^2; for the unbiased cell, both electrodes have the same area), and t is the illumination time (h).

The solar-to-chemical conversion (SCC) efficiency for H_2O_2 production is defined as:

$$SCC = \frac{\Delta G \times (n_{H2O2,anode} + n_{H2O2,cathode})}{P_{solar} \times A_{cell} \times t} \times 100\%$$

where ΔG = 117 kJ mol^{-1} is the standard Gibbs free energy of H_2O_2 formation from H_2O and O_2 (averaged for the two half-reactions), n is the total amount of H_2O_2 (mol) produced at both electrodes, P_{solar} is the solar power density (100 mW cm^{-2} for AM 1.5G; measured value for outdoor test), and A_{cell} is the illuminated area (same as electrode area, since both electrodes are illuminated in our tandem configuration). For outdoor tests, we used the measured average sunlight intensity (≈72 mW cm^{-2} on the test day).

The areal production rate is calculated based on the total illuminated area (anode + cathode, both illuminated in the tandem configuration). For the 20 cm^2 electrodes, total illuminated area = 40 cm^2, giving a rate of 19.1 μmol cm^{-2} h^{-1}; for the 36 cm^2 electrodes, total illuminated area = 72 cm^2, giving a rate of 15.9 μmol cm^{-2} h^{-1}. (If expressed per single electrode area, the values would be twice as high: 38.2 and 31.8 μmol cm^{-2} h^{-1}, respectively.) The SCC efficiency was calculated using the Gibbs free energy of H_2O_2 formation (117 kJ mol^{-1}) and the measured total H_2O_2 amount. Under 0.72 sun natural sunlight, the SCC values are 0.86% for the 20 cm^2 electrodes and 0.72% for the 36 cm^2 electrodes **(Table R2)**.

2) Evaluation against disinfection benchmarks: The H_2O_2 concentrations achieved in the scaled-up tests (7.64 mM = 260 mg/L; 11.94 mM = 406 mg/L) far exceed the typical thresholds required for effective water disinfection. For example, a concentration of 25-50 mg/L H_2O_2 is sufficient to achieve >99.9% inactivation of E. coli within 30-60 min in the dark.[3-6] Our concentrations are 5-16 times higher than this benchmark, confirming that the system can generate H_2O_2 at levels that are practically useful for disinfection without any further concentration step.

Table R2 Areal production rates and SCC efficiencies.

Electrode area (each)	Current (mA)	Combined FE (%)	$Yield_{H2O2}$ (mM)	Areal production rate (μmol cm^{-2} h^{-1})	SCC (%)
20 cm^2	24.78	165.38	7.64	19.1	0.86
36 cm^2	37.54	163.37	11.94	15.9	0.72

References

[1] Wang, L., Guo, F., Ren, S., Gao, R.-T., Wu, L. Unbiased photoelectrochemical H_2O_2 coupled to H_2 production via dual Sb_2S_3-based photoelectrodes with ultralow onset potential. *Angew. Chem. Int. Ed.* **63**, e202411305 (2024).

[2] Wang, L., Wu, Y., Mao, S., Zhou, J., Zhang, Y., Zheng, X., Wu, X., Xu, H. Dual-Functional Catalyst of Amorphous TiO_2 Embedded in Mesoporous Carbon Hollow Spheres for H_2O_2 Electrosynthesis. *Adv. Mater.* **37**, e08326 (2025).

[3] Gao, R.-T., Gao, Z., Nguyen, N. T., Chen, J., Liu, X., Wang, L., Wu, L. Photoelectrochemical production of disinfectants from seawater. *Nat. Sustain.* **8**, 672-681 (2025).

[4] Jiang, C., Fei, Y.-F., Xu, W., Bao, Z., Shao, Y., Zhang, S., Hu, Z.-T., Wang, J. Synergistic effects of Bi_2O_3 and Ta_2O_5 for efficient electrochemical production of H_2O_2. *Appl. Catal. B* **334**, 122867 (2023).

[5] Zhang, M.-D., Huang, J.-R., Liang, C.-P., Chen, X.-M., Liao, P.-Q. Continuous Electrosynthesis of Pure H_2O_2 Solution with Medical-Grade Concentration by a Conductive Ni-Phthalocyanine-Based Covalent Organic Framework. *J. Am. Chem. Soc.* **146**, 31034-31041 (2024).

[6] Ye, Y. -X., Pan, J., Shen, Y., Shen, M., Yan, H., He, J., Yang, X., Zhu, F., Xu, J., He, J., Ouyang, G. A solar-to-chemical conversion efficiency up to 0.26% achieved in ambient conditions. *Proc. Natl. Acad. Sci. U.S.A.* **118**, e2115666118 (2021).

We really thank all the reviewers for the suggestive comments. We believe that the quality of the manuscript will be greatly improved after revision.

Reviewer #1:

After the revision, this work could be accepted.

We thank Reviewer 1 for the encouraging evaluation and for recognizing the novel contribution of our bias-free tandem PEC system.

Reviewer #3:

I appreciate the author's efforts for addressing all the comments raised during the review. no further comments.

We thank Reviewer 3 for the positive comments of our manuscript. We appreciate the reviewer's comments in evaluating our work.

Reviewer #5:

The authors have carefully revised their manuscript according to the suggestions from the reviewers and addressed all the comments completely. After revision, the overall quality of the manuscript is improved and meets the standard, thus, I would like to recommend the manuscript to be accepted for publication.

We thank Reviewer 5 for the positive comments. We are grateful for the constructive feedback that helped improve the quality of our study.

Reviewer #2:

We thank the reviewer 2 for the positive comments on our manuscript. We have made the suggested revision.

General Comment: The authors have produced a novel bias-free tandem photoelectrochemical (PEC) system for sustainable hydrogen peroxide (H_2O_2) synthesis. By strategically integrating a Zn-TiO_2/$BiVO_4$/WO_3 photoanode and a Ru:CuO/Nb-CBO photocathode, the authors successfully elucidate the origin of highly selective H_2O_2 production, demonstrating how heterojunction engineering and precise element doping effectively suppress competing four-electron pathways and stabilize key *OOH intermediates. The impressive practical demonstrations, including a total Faradaic efficiency exceeding 160% in a scalable, membrane-free outdoor setup and its application for rapid

bacterial inactivation, make this work highly commendable. This research is likely to capture the attention of a wide readership within the renewable energy and photoelectrocatalysis fields of the journal. Notwithstanding, to ensure acceptance, the authors need to deal with the following minor considerations:

1. The authors report onset potentials for BVO, BVO/WO_3, TiO_2/BVO/WO_3, and Zn-TiO_2/BVO/WO_3 ranging from 0.31 to 0.45 V_{RHE}. However, the potential window selected for capacitance measurements (0.2-0.4 V_{RHE}) overlaps with these Faradaic onset values. Since ECSA calculations must be conducted in a strictly non-Faradaic regime, this discrepancy may compromise the accuracy of the results. The authors should clarify this mismatch, re-evaluate their definition of onset potential, or adjust the potential window used for ECSA determination.

Response: We thank the reviewer for the careful observation. We deeply apologize for the potential inaccuracy in our initial ECSA measurements due to the overlapping potential window. We have re-measured the electrochemical surface area (ECSA) for all photoanodes using a strictly non-Faradaic potential window of 0.1-0.3 V_{RHE}. Zn-TiO_2/BVO/WO_3 exhibits a specific capacitance of 19.75 μF cm^{-2}, two as high as that of BVO (9.60 μF cm^{-2}), confirming a great number of electrochemically active sites for rapid interfacial charge transfer (**Fig. R1**).

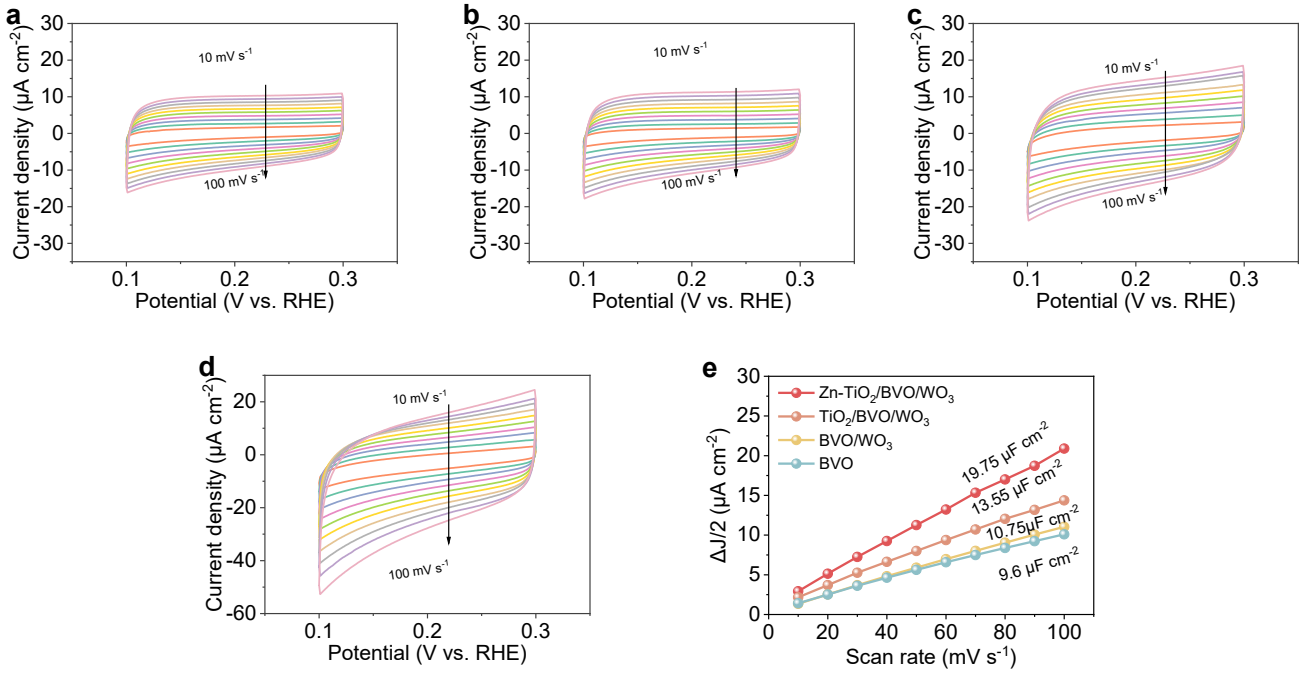

Fig. R1 a-d Cyclic voltammetry curves of **a** BVO, **b** BVO/WO_3, **c** TiO_2/BVO/WO_3, and **d** Zn-TiO_2/BVO/WO_3. **e** Relative electrochemical surface areas for the linear relationship.

2. While the schematic in Fig. 4a and the scaled-up system are presented as membrane-less, the data for the small-scale system in Fig. 4c was obtained using a proton exchange membrane (PEM). To ensure the validity of the proposed membrane-free architecture, the authors need to provide stability data for the small-scale cells (1 and 2 cm^2) under membrane-less conditions, matching the setup of the scaled-up system and schematic illustration.

Response: Thank you for the valuable comments. We have now performed additional stability tests for small-scale cells under membrane-free conditions. For 1 cm^2 and 2 cm^2 cells (no membrane), the unbiased tandem system maintained stable photocurrent and H_2O_2 production for over 2 h, with total Faradaic efficiencies (FE) of 167.12% and 165.23%, respectively (**Fig. R2**). The membrane-free operation at small scale now directly matches the configuration of the scaled-up outdoor system and the schematic in Fig. 4a.

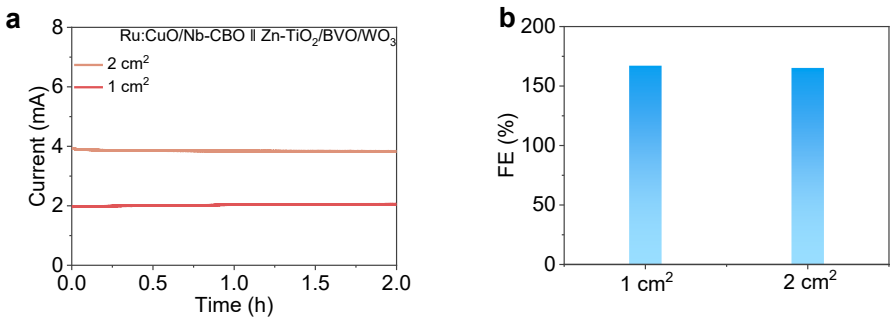

Fig. R2 a Chronoamperometry of unbiased Ru:CuO/Nb-CBO ‖ Zn-TiO_2/BVO/WO_3 (no membrane). The surface areas of photoelectrodes are 1 cm^2 and 2 cm^2. **b** H_2O_2 FEs for corresponding cells (no membrane).

3. Despite the authors' efforts to suppress H_2O_2 degradation at both the photoanode and photocathode, H_2O_2 is inherently unstable due to its low thermodynamic barriers and facile kinetics toward both electrochemical oxidation and reduction. Given this bipolar instability, the system's ability to accumulate the product is likely limited. The authors should, therefore, determine the maximum attainable H_2O_2 concentration that this specific system can accommodate before decomposition rates offset production.

Response: Thank you for this important suggestion. We performed a long-term accumulation experiment under unbiased conditions in a membrane-free cell (1 cm^2 electrodes) (**Fig. R3**). The H_2O_2 concentration was monitored over 10 h. The results show that the concentration increases steadily during the first 8 h, reaching approximately 500 μmol, and then gradually stabilizes. The maximum

attainable H_2O_2 concentration after 10 h is about 500 μmol.

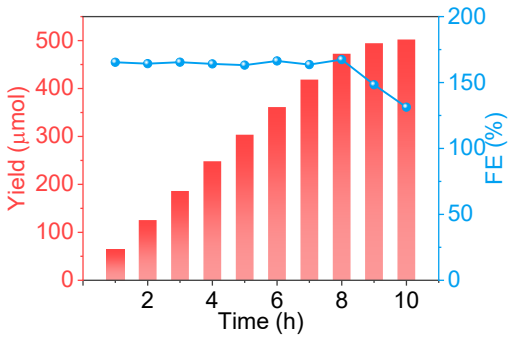

Fig. R3 Accumulated H_2O_2 yields and FEs on unbiased Ru:CuO/Nb-CBO ‖ Zn-TiO_2/BVO/WO_3 in a membrane-free system during 10 h operation. The surface areas of photoelectrodes are 1 cm^2.

4. The statement "Gas chromatography measurements indicate that Zn-TiO_2/BVO/WO_3 exhibits the highest selectivity for H_2O_2 production at 0.6 V_{RHE}, releasing the lowest amount of O_2 among these photoanodes" in page 8 is quite confusing because GC measures only O_2. Authors need to clarify this statement and indicate that FE of H_2O_2 plus O_2 equals ~100%.

Response: We thank the reviewer for the constructive comments. We deeply apologize for this confusion. We have re-measured the FEs and selectivities of O_2 for all photoanodes and obtained consistent results **(Fig. R4)**. The sentence has been revised for clarity. It now states: "Gas chromatography measurements were used to quantify the evolved O_2. At 0.6 V_{RHE}, Zn-TiO_2/BVO/WO_3 releases the lowest amount of O_2 among all photoanodes, exhibiting the highest selectivity for H_2O_2 production (**Fig. 2d**)." The sum of the Faradaic efficiencies and selectivities for H_2O_2 production and O_2 evolution is approximately 100% for each photoanode, confirming that $2e^-$ WOR (H_2O_2) and $4e^-$ OER (O_2) are the only competing pathways.

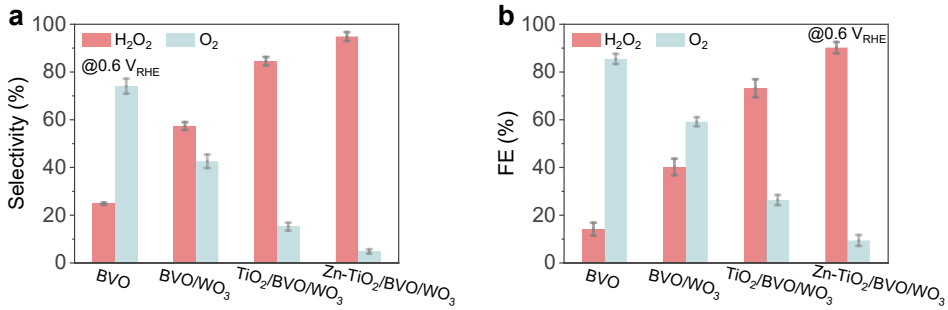

Fig.R4 a Selectivities and FEs of of H_2O_2 and O_2 at 0.6 V_{RHE} for BVO, BVO/WO_3, Ti-O_2/BVO/WO_3, and Zn-TiO_2/BVO/WO_3 photoanodes.

5. There are typo. The authors need to correct it. For example: 'selecitivities' in page 9, 'photoccathodes' in page 25, 'Ar2', in Fig. S18.

Response: We thank the reviewer for the comments. All have been corrected: "selecitivities" → "selectivities", "photoccathodes" → "photocathodes", and "Ar_2" → "Ar". We have carefully double-checked the whole manuscript and supplementary information.

Reviewer #4:

We thank the reviewer 4 for the positive comments of our manuscript. We have made the suggested revision.

The authors have accurately revised the manuscript in accordance with the reviewer's comments. In addition, most of the reviewer's questions have been addressed in the revised version. Therefore, I feel that this manuscript has the potential to be published in Nature Communications.

However, I feel that it would be preferable to make the following minor revision:

The authors should add the concentration (or amount) of the pre-added H_2O_2 (0.5 M) to the caption of the newly added Supplementary Fig. 43(c).

Response: We thank the reviewer for the useful comments. The concentration of pre-added H_2O_2 in the decomposition control experiment was 0.5 M. We have added this information in the caption of Supplementary Fig. 43(c) accordingly.